Study of percolation phenomena in ironmaking by DEM

Master's thesis

OMORODION JEFFERY

Supervisor: Prof. Henrik Saxén

Thermal and Flow Engineering Laboratory

Faculty of Science and Engineering

Åbo Akademi University

Turku, Finland. May 2019.

SUPERVISORS

Professor Henrik Saxén

Thermal and Flow Engineering laboratory,

Åbo Akademi University, Åbo, Finland.

Dr Timo Paananen

SSAB Ab Europe,

Raahe, Finland

PREFACE

My sincere appreciation goes to SSAB Europe for providing this thesis opportunity through the funding made available, my supervisors both from the laboratory Prof. Henrik Saxen for valuable intellectual discourse and from the industry, Dr Timo Paananen and M.Sc. Olli Mattila. My gratitude is extended to Alf Hermanson for those numerous times where he had to help with issues regarding software and PC and Vivéca Sundberg for all the administrative help. To my parents and extended family who sacrificed everything and gave their all for me to be here today. I say a big thank you to all of my classmates who assisted me along this journey, especially Taimoor and Riza, who were there in difficult times. To 'dem my real sure guys' Gerald, Raph, Justin, Dola. 'I hail una ooo' to Umarita-Yumi my office and course mate for all those friendly disturbances, assignments, group work, friendly and intellectual discourse. To Rasmus for sharing some experimental results. To all those who have in one one way or the other contributed to my journey thus far, I say a huge thank you.

Tack tack!

Turku, Finland. May 2019

Jeffery Omorodion

SVENSK SAMMANFATTNING

Ett växande behov av stål i världen har ökat behovet av råjärn, vilket kräver en ökning av produktionskapaciteten och –effektiviteten hos masugnar som reducerar och smälter järnmalm. Vid hantering av råmaterial för masugnsprocessen och under produktionen då beskickningsmaterialen sjunker genom ugnen sker oönskad segregation och perkolation av de partikelformiga materialen, främst agglomererade järnoxider (sinter eller pelletar) och koks. I stora siloer för lagring av pelletar kan den minsta fraktionen (pelletkärnor och ”stoft”) anrikas och tidvis kraftigt strömma ut okontrollerat p.g.a. komplexa strömningsmönster. I masugnen kan järnbärare, framför allt pelletar, perkolera i ett underliggande kokslager och minska dess porositet och permeabilitet, vilket påverkar tryckfallet för och fördelningen av gasen som strömmar uppåt genom bädden. Detta kan i extrema fall leda till svåra processtörningar eller t.o.m. avbrott i produktionen.

I föreliggande avhandling studeras perkolering beräkningstekniskt med den s.k. diskreta elementmetoden (eng. discrete element method, DEM). Detta angreppssätt har fördelen att ge insikt i och en visuell bild av partiklarnas komplexa strömning, som inte kan erhållas i den verkliga processen p.g.a. ogenomskinlighet samt svåra omständigheter (hög temperatur, skadliga gaser, stort slitage). Inte heller i småskaleförsök kan man undersöka partikelbäddars inre utan att påverka bäddens struktur eller strömning. Under de senaste årtionden har DEM utvecklats både metod- och beräkningsmässigt hand i hand med att datorerna blivit snabbare, vilket idag gjort det möjligt att angripa mer realistiska problem. Trots detta kräver metoden avsevärd beräkningskraft och stora mängder datorminne, varför de system som studeras i regel måste skalas ner för att man skall erhålla en lösning inom rimlig tidsram.

Avhandlingen studerade genom simulering olika faktorer som påverkar perkoleringen genom att simulera hur pelletar i ett ovanliggande lager tränger in i ett kokslager, då lagren långsamt sjunker ner i ett cylindriskt eller koniskt schakt. Systemet som studerades har en diameter omkring 30 cm och lagren rör sig nedåt omkring 50 cm. Partiklarna har storlekar in området 5-30 mm, där pelletarna är sfäriska och små medan koksen har en oregelbunden form och är större. En oregelbunden partikelform skapades numeriskt genom att koppla samman (”klumpa ihop”) mindre sfäriska partiklar som delvis överlappade varandra. Simuleringen omfattar en generering av de två materiallagren genom att slumpmässigt bilda partiklar som faller och samlas inom domäner, vilka sedan tillåts kollapsa för att bilda en bädd bestående av ett

materiallagerpar. Denna bädd får härnäst sjunka långsamt (med angiven hastighet), varvid en virtuell ”låda” i kokslagret följer med hur många pelletar som strömmat in.

Storleksförhållande för partiklarna, hastigheten med vilken partikellagren sjunker och bäddvibrationer befanns påverka omfattningen av pelletars perkolering i ett kokslager. För fall där partikelbädden vidgades (på ett masugnsschaktliknande sätt) ökade perkoleringen dramatiskt och ju mer desto snabbare bäddens tvärsnitt växte. Däremot befanns inte pelletegenskaper såsom koefficienter för statisk friktion eller rullfriktion ha någon större betydelse för perkoleringen. Vid schaktväggen var partiklarnas strömning begränsad och materiallagrens rörelse hämmades, vilket ledde till U-formade profiler för lagrens gränssnittsytor. Speciellt befanns koksens rörelse hämmas av väggarna, troligtvis p.g.a. dess oregelbundna form. Man bör dock notera att systemen som studerades var kraftigt nedskalade i avseende på domängeometrin, varför partiklarnas diametrar är överdrivna i jämförelse med schaktdiametern.

För siloerna som simulerades undersöktes hur den minsta storleksfraktionen i en blandning av olika stora partiklar beter sig vid periodisk chargering och partiell tömning. En nedskalad silo och partiklar av tre storlekar studerades. Silon fylldes först varefter cykler av tömning och chargering följde. Den minsta partikelstorlekens andel i siloinnehållet, i den nedre delen av silon och i utströmmen uppföljdes. Effekten av att tömningen skedde genom ett eller flera kvadratiska hål i den plana bottnen av silon undersöktes även. Resultaten för försök med ett begränsat antal fyllnings/tömnings-cykler visade att andelen fina partiklar ökade i utströmmen medan andelen i bädden minskade med tiden. Däremot ökade andelen i bäddens nedre del. Detta visar att partiklarna via perkolering vandrar nedåt och gradvis fyller silons undre delar med fint material. Tyvärr tog simuleringarna så lång tid i anspråk att det inte gick att simulera förloppet tillräckligt länge för att nå ett stationärtillstånd (om ett sådant överhuvudtaget nås). Simuleringsresultaten visade överensstämmelse med observationer i driften av verkliga pelletsiloer.

Några faktorer som kunde undertrycka perkolering diskuterades även. Det enklaste sättet vore att öka på storleksförhållandet mellan små och stora partiklar, men detta kan knappast tillämpas av olika praktiska skäl. Dock kunde man skapa gränssnitt mellan lager med olika lokala egenskaper som kunde minska på perkoleringens omfattning. I siloer kunde effekterna av en

oönskad perkolering eventuellt reduceras om man lyckas hålla bäddens ytnivå möjligast konstant, då plötsliga variationer i utströmmen med denna metod kan begränsas.

Avhandlingens arbete visar att DEM är en slagkraftig metod som med fördel kan utnyttjas för att får insikter i hur partikelflöden utvecklas under olika omständigheter och i olika geometrier. Metoden gör det möjligt att man betraktar enstaka partiklar och deras lägesmässiga rörelse och rotation, att undersöka förhållandena längsmed olika plan, varför man kan få en detaljerad bild av förloppen. Emellertid kräver metoden att partikelformerna kan beskrivas rimligt och att man kan uppskatta tillräckligt noggranna värden för olika fysikaliska parametrar som beskriver partiklarnas egenskaper. Till metodens nackdelar hör också att beräkningarna ofta blir tunga och att beräkningstiden växer kraftigt med antalet partiklar i systemet. Därför måste man göra kompromisser (t.ex. i avseende på partikel- vs. systemstorlek) och dessa måste beaktas när resultaten tolkas. Trots dessa begränsningar konstaterades metoden vara väl lämpad att studera komplexa fenomen såsom partikelsegregering och perkolering vid hantering av styckformat material.

Jeffery Nosakhare Omorodion

ABSTRACT

Increasing demand for steel has prompted an increase in production capacities for hot metal and a need to improve the efficiency in the blast furnace operation. In the handling of the raw materials used in ironmaking, and during their charging and descent in the blast furnace, undesired segregation and percolation phenomena may occur. In large silos used for intermediate storage, smaller fines of the material may accumulate and purge non-uniformly due to complex particle flow mechanics. In the blast furnace, iron ore percolation into underlying coke layers can reduce the voidage of the coke layer, which affects the pressure loss and distribution of the gas. In extreme cases, this may contribute to process disturbances in the furnace.

This thesis studies percolation computationally using the discrete element method (DEM). This simulation approach has the advantage of providing visual and graphical insight into percolation in the system studied, which cannot be obtained from the system due to the opacity of the granular material involved and the hostile environment of the real system. Over the years, the discrete element method has also evolved, making it possible to study more realistic systems today, partly due to improvement and parallelisation of the software and the growing computational speed. As the application of the technology is still limited by computational resources available, the systems studied must be down-scaled to make the solution feasible.

The effects of different materials and process parameters on percolation were investigated. Size ratio, descent velocity, vibration amplitude and frequency were found to enhance the percolation of pellets in underlying coke beds. Some ways to reduce the extent of percolation were also briefly discussed, the most important one being reducing the size ratio between the large and small particles. In silos, suppressing large changes in the filling and discharge heights may be a remedy.

Keywords: Segregation, percolation, discrete element method, furnace, silo, simulation

ABBREVIATIONS

DEM	Discrete Element Method
WSA	World Steel Association
BF	Blast furnace
CAD	Computer Aided Design
COF	Coefficient of Friction

TABLE OF CONTENTS

LIST OF FIGURES

LIST OF TABLES

1 INTRODUCTION

Steel is a multifunctional material that forms the backbone of developed societies. The steel demand is continuously growing in the world and, in 2017, it exceeded 1600 million tons. Data from WSA Steel Statistical Yearbook (2018) showed that, in 2017, Finland produced around 4 million metric tons of crude steel making it the 36th largest producer in the world. In ore-based steelmaking, the blast furnace forms the most central process unit, where iron ore is reduced and melted to hot metal that is refined into steel in downstream processing units.

Qiu et al. (2017) define a blast furnace as a large counter-current moving bed reactor involving complex mass transfer, heat transfer, momentum transfer, and chemical reactions between descending solid materials and ascending gas. The particulate burden, consisting mainly of preprocessed ore (sinter or pellets) and the primary reductant and energy source, coke, is charged from above to enter the process and descend by gravity. According to Wei et al. (2017), chemical reactions between raw material and gas in the furnace are determined primarily by the burden distribution, especially the radial distribution of pellet/sinter and coke.

There is no gainsaying that much work has been done as regards unravelling the mysteries behind this particulate material which on its own could be regarded as a state of matter. In the blast furnace, the discontinuous granular material is prone to compaction, dilation, expansion and segregation which alters the properties of the bed.

Percolation is a form of segregation that can occur in any unit operation involving the handling of granular materials. It simply can be defined as a de-mixing process, where fine or smaller particles flow through interstices of a bed of coarse or larger particles. Although it may have a positive influence on some processes, in the case of a blast furnace it often causes adverse effects by creating dense regions, and by introducing undesired dynamics and disturbances into the production processes. Percolation is enhanced when the particle body force on the discontinuous granular material is greater than the particle-particle force, mainly as a result of gravitational forces on particles. Hence, percolation does not occur to a substantial extent for cohesive materials.

Percolation in the blast furnace affects the particulate microstructure which, in turn, influences the material properties such as voidage distribution, and consequently gas distribution, which is relevant to fluid flow and an essential factor in the furnace kinetics, which will inadvertently affect chemical reactions and heat transfer.

Pierce (2004) noted that for particles that are smaller than the minimum interstices between larger particles, percolation could occur spontaneously, while particles that are larger than the minimum interstices may only percolate if the bed is disturbed in some way (e.g. through shearing, vibration) or, as in this thesis, by burden descent and strain. There is a need to adequately understand and control the dynamics in the blast furnace, to which percolation in some way contributes.

Fayed and Otten (1997) and Rosato et al. (2002) identified the differences in physical and mechanical parameters of materials that could influence particle segregation during any handling process, including particle size and distribution, density, shape, morphology, structural properties and rheology of particle packing, contact friction, elasticity, brittleness, ability to absorb moisture, size enlargement, size reduction, electrostatic charges, vibration, intensity and displacement of motion, and magnetic properties. The present work will study the effect of some of the parameters on segregation in the moving blast furnace burden.

Experimental measurements in the furnace are complicated due to the opaque nature of both granular materials and furnace wall, and more so, it is a high-temperature process with an operating temperature that locally may exceed 2000^{o}C.

The particle size ratio in blast furnaces is usually quite small (ranging between 2 and 6), and the particles, being pre-screened to remove fines, often have a relatively narrow size distribution. Hence, spontaneous inter-particle percolation does not usually occur. Once the material descends into the stack region, where the diameter of furnace increases, it experiences a strain causing failure zones coupled with the friction provided by the wall, which leads to the creation of new void. The present study is primarily concerned with studying interparticle percolation induced by burden descent and from the strain experienced in the stack.

Another problem studied in the thesis is the dynamics of fine particles in a pellet bin. Due to the impact force on the material as a result of the falling height and also percolation, the

concentration of fines may increase in certain regions of the bin, and the cycling charging and discharging of the bin may further aggravate the problem. Even though the pellet fines are generally sieved before the pellets are transported to the blast furnace, a too high share of fines can still be detrimental. If a high portion of fines is removed, there may not be enough burden material left for the furnace, so the hot metal production rate must be decreased. However, allowing for more fines makes it necessary to manage the consequences that come with maldistribution of the reducing gas in the furnace.

The bed descent is due to the void created in the blast furnace partly by combustion and gasification of coke close to the tuyeres and the softening and melting of the ores. The descent of the burden is also affected by percolation, which is often an undesired feature. Qualitative analysis of segregation does not provide sufficient information to be able to address the problem. Therefore, it is essential and beneficial to carry out a quantitative investigation of percolation. Understanding, quantifying and controlling the mechanisms would make it possible to attain a better controlled (quasi) steady-state operation of the blast furnace, with more uniform burden descent and residence time distribution of the burden, as well as improved indirect reduction, which are prerequisites of a smooth supply of hot metal with uniform quality to the steelmaking process.

To understand the concept of percolation, numerous researchers have carried out studies under different conditions, e.g., in hopper charging and discharging. Some examples are given below.

Yu and Saxén (2014) studied the effect of particle shape on segregation in a hopper and during discharge using the discrete element method. Scott and Bridgwater (1975) studied strain-induced inter-particle percolation. Yu and Saxén (2010) studied both through experiments and simulations the size segregation of ternary size pellets during the discharging process of a hopper model. Chou et al. (2009) studied the effect of an insert to reduce the quasi-stagnant zone next to the hopper wall in an asymmetrical bin hopper. Zhu and Yu (2005), using the averaging technique, studied the macroscopic dynamic behaviour of granular flow in a cylindrical hopper with a flat bottom. Wu et al. (2009) studied the dependence of flow behaviour on particle diameter distribution in silo and the use of an insert. Ketterhagen et al. (2008) used periodic boundary conditions in the discrete element method to investigate the segregation of granular materials during discharge from a wedge-shaped hopper.

In most of the previous studies of percolation, whether experimental or computational, only the percolating particles had a downward component of velocity and the parking or burden material usually was stagnant. In the cases where both had descent velocities like in a hopper or chute, percolation was not usually studied.

In this thesis, cohesionless material (coke and iron pellets) are studied. The iron pellet has a uniform shape and size, hence is regular, while coke is composed of particles of different shapes and size and is hence irregular. The work focused mainly on studying how pellets charged on a coke layer percolate into the coke layer as the layers descend. The effect of material properties on percolation was also studied. Different ways of mitigating the effect of pellet percolation were also analysed. The simulation results were validated by comparison with previous results published in the literature by other researchers.

The effect of multiple filling and discharging of a small-scale pellet bin was also studied by DEM, where the emphasis was put on analysing whether finer particles are accumulated and depleted during the cyclical operation.

General conclusions were finally drawn on how the result could be applied in practice.

2 BLAST FURNACE OPERATION

2.1 Process Description

The blast furnace is charged with alternating layers of coke and the iron ore–bearing burden. Air, also known as blast, is blown into the lower part of the blast furnace via nozzles, tuyeres. Coke and injected reductants are consumed and gasified in front of the tuyeres, producing reducing carbon monoxide; this gasification inadvertently creates voidage, which is the driving forces for burden descent in the blast furnace.

The gas that forms in the combustion region, raceway, has a high temperature of 2100-2300 °C, and it gradually cools as it ascends, heating the coke in the bosh/belly area and the burden in the shaft zone of the blast furnace. When the iron-bearing burden melts, extra voidage is created, which also contributes to burden descent. After melting, hot metal and slag produced from the iron ore dribble down through the coke bed into the hearth. They are then removed by casting through the taphole. The dripping hot metal also consumes carbon, because below the melting zone, coke is consumed for carburisation of the iron as well as in the direct reduction reactions.

The ore burden layers account for the majority of resistance to gas flow, and the reduction process takes place within these layers. The permeability of the ore burden is determined mainly by the particle size distribution, and particularly by the share of small particles (fines). Geerdes et al. (2015) list factors that affect the amount of fines. They are the screening efficiency in the stock house, the physical degradation during transport and charging, the method of burden distribution used, and the low-temperature degradation properties of the burden. An example of the appearances of burden material used in the blast furnace is presented in Figure 1 (Geerdes et al. (2015)).

Figure 1: Images presenting the shapes of furnace feed materials (Geerdes et al., 2015)

Fines are burden material with a size less than 5 mm. There are two sources of fines: those that are directly charged into the furnace, and those that are produced in the process. During charging, fines in the burden material tend to concentrate at the point of impact on the burden surface. Proper screening of burden materials before charging is, therefore, a key issue, but if the share of fines is high, it has a disadvantage of sometimes leaving behind less material for the furnace.

After the iron ore is reduced and melted in the furnace the product from the reaction, hot metal, is transported in liquid state to the steel plant where it is further processed into steel by removing elements such as sulphur, silicon, carbon, manganese and phosphorous. Waste slag produced from the gangue of the ore burden and the ash of coke and coal is often granulated and can be used in the production of cement. Hot metal and liquid slag remain separate from each other since they do not mix and with the slag floating on top of the denser iron. This physical difference is exploited in the cast house where the iron can then be separated from the slag. Geerdes et al. (2015) describe the process and auxiliary facilities (cf. Figure 2) as well as the zones in a modern day blast furnace, as depicted in Figure 3.

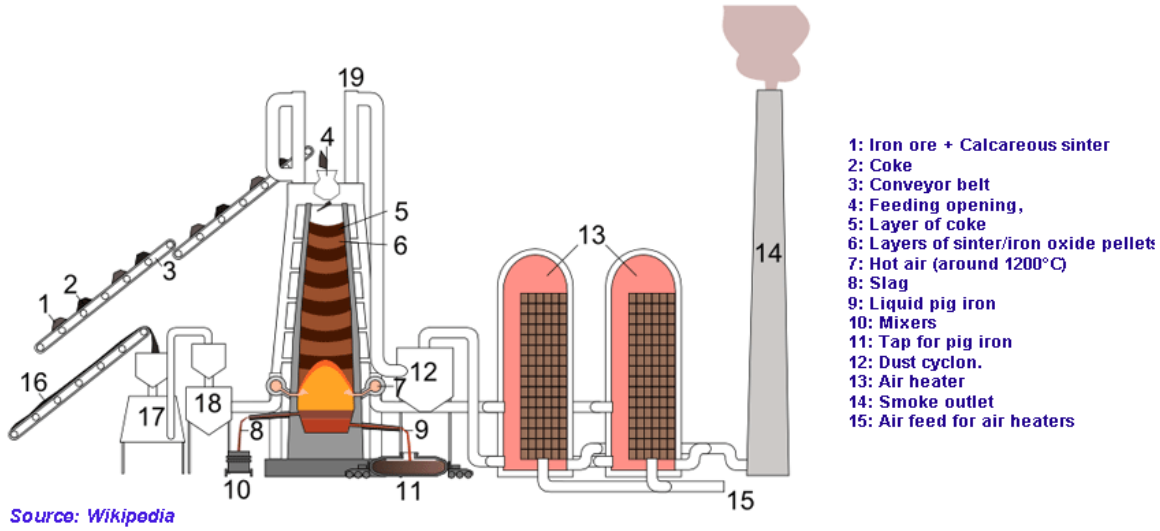

Figure 2: Blast furnace process flow diagram

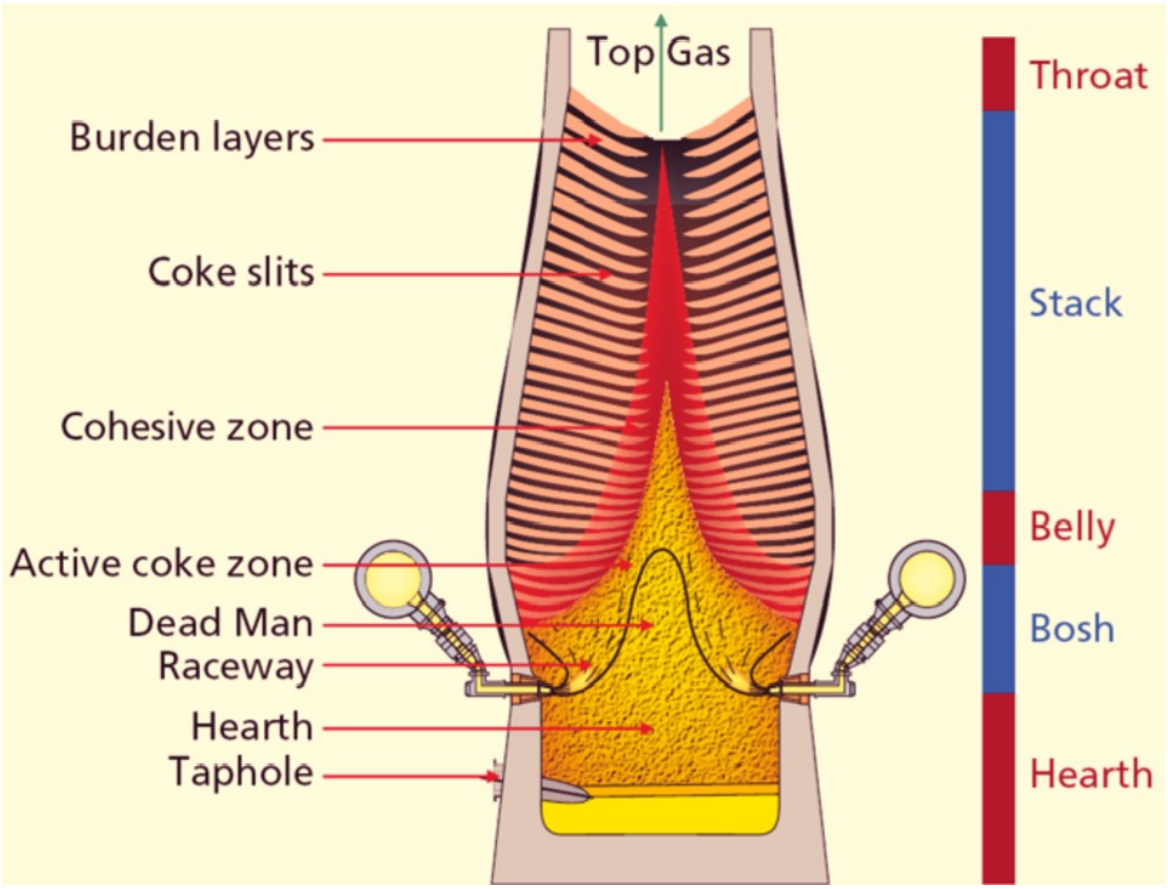

Figure 3: Slice view of zones in a blast furnace (Geerdes et al., 2015)

The area where ore begins to soften and melt is called the softening–melting or cohesive zone. The region directly below the cohesive zone where there is only coke and liquid iron and slag is known as the "active coke" or dripping zone. In the hearth of the furnace, a stable pile of coke is formed which is termed the dead man. The stack is where the ores are heated and the reduction reactions start, in the bosh parallel or belly the reduction is completed, and the ores are melted down, and finally the hearth is the place where the molten material is collected and is cast via tapholes.

2.2 The Process Chemistry

A brief description of the chemistry in the blast furnace is provided here. An exothermic reaction occurs between the preheated blast whose temperature is 1100-1200°C and the coke. The bast oxidises the carbon content of the coke to produce carbon monoxide while also releasing heat.

$$2\ C_{(s)} + O_{2\ (g)} \rightarrow 2\ CO_{(g)}$$

The hot carbon monoxide gas produced thus becomes the reducing agent for the iron ore in the iron production process. It reacts with the iron oxide to produce carbon dioxide and metallic iron, in molten form in the lower regions of the blast furnace. There are temperature profiles in both the horizontal and vertical direction of the furnace which affect the kind of reactions taking place at different parts of the furnace. The iron ore is reduced in several steps as the burden descend. The temperature at the top usually have values that fall between 200 °C and 700 °C. Hence, the iron oxide is partly reduced to iron (II, III) oxide Fe_3O_4.

$$3\ Fe_2O_{3(s)} + CO_{(g)} \rightarrow 2\ Fe_3O_{4(s)} + CO_{2(g)}$$

Further down in the furnace at temperatures around 850 °C, iron (II, III) is further reduced to iron (II) oxide as shown below:

$$Fe_3O_{4(s)} + CO_{(g)} \rightarrow 3\ FeO_{(s)} + CO_{2(g)}$$

As the material moves downward from the top towards the reaction zone, the ascending gases, heat the burden material. Limestone in the burden decomposes to carbon dioxide and calcium oxide:

$$CaCO_{3(s)} \rightarrow CaO_{(s)} + CO_{2(g)}$$

The calcium oxide generated from the decomposition reacts with various acidic impurities in the iron, especially silica, to produce slag which is mainly calcium silicate, $CaSiO_3$:

$$SiO_2 + CaO \rightarrow CaSiO_3$$

As the iron (II) oxide moves further downwards towards high-temperature areas, at around 1200 °C, it is reduced further to metal iron:

$$FeO_{(s)} + CO_{(g)} \rightarrow Fe_{(s)} + CO_{2(g)}$$

In the high-temperature region, the carbon dioxide formed in the reaction above undergoes reduction to carbon monoxide by the coke in the burden

$$C_{(s)} + CO_{2(g)} \rightarrow 2\ CO_{(g)}$$

The highly temperature-dependent equilibrium of the Boudouard reaction controls the gas composition in the lower furnace. At temperatures above 1000 °C, practically all carbon dioxide is converted to carbon monoxide if it encounters coke. Therefore, at the high temperatures experienced in the melting and bosh zone of the blast furnace, only carbon monoxide is present. At temperatures below 500 °C, all carbon monoxide (CO) tends to decompose into $C+CO_2$. This carbon produced is very fine, and it is called the Boudouard carbon. The formation of carbon from CO slows down at lower temperatures, and it becomes prominent at temperatures around 500 – 550 °C.

$$2CO \rightleftharpoons CO_2 + C$$

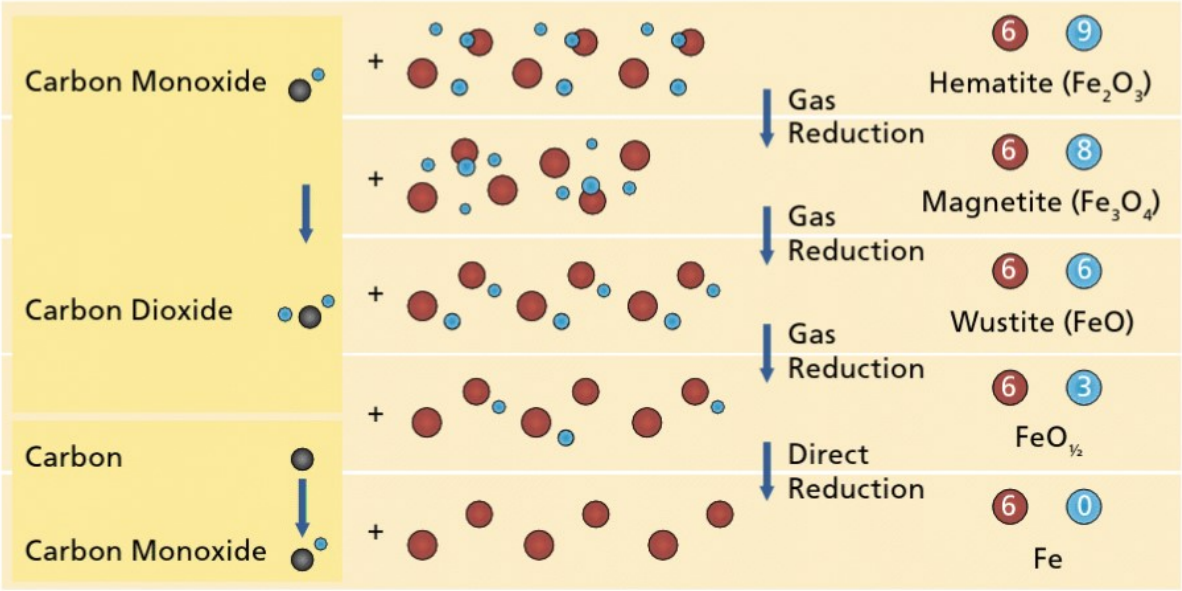

Figure 4: Overview of the reduction of iron oxides. Black dots represent carbons atoms, blue dots oxygen atoms, and red dots iron atoms (Geerdes et al., 2015).

2.3 Coke in the Blast Furnace

Coke is the only solid material below the melting zone, so the coke structure supports the total weight of the burden column. The coke material is also responsible for producing the reducing gases, which, in turn, provide heat to melt the burden. It also provides the carbon needed for carburization of the hot metal. The carburization plays an important role as the dissolved carbon lowers the melting point of the hot meal, and since the carbon acts as an energy source in the downstream processes (e.g., basic oxygen furnace). The coke used in blast furnace should be strong and relatively inert since gasification and reaction at "too" low temperatures would lead to degradation and lower permeability. The coke may also be weakened as it is charged into the process.

Screening the coke fines in the stock house will increase the permeability of the resulting coke bed in the blast furnace. The smallest fraction (< 5 mm) should not be charged into the blast furnace, but the intermediate fraction can be added to the ore layer to increase its permeability. This coke is usually referred to as "nut coke". If very coarse coke particles are charged into the furnace, the large void could be filled by smaller ore particles, resulting in the formation of

thick mixed layers at the coke–ore interface yielding low permeability. Small coke layers may be charged upon large coke to prevent the formation of excessive mixed layers.

2.4 Burden Descent and Gas Flow Control

There is a downward movement of the burden, i.e. descent in the blast furnace from top to bottom, while the reducing gas ascends from bottom to top. The burden surface descends with an average speed of 8-15 cm/min, and, the velocity of the gas in the furnace is much higher, but still quite modest, with a vertical component of a few meters per second (Geerdes et al., 2015). The burden descent is driven by voidage created lower down in the process. Coke combustion in front of the tuyeres leads to the formation of voidage. As the hot reducing gas rises in the furnace, the iron-bearing material is heated, reduced to finally melt, which creates voidage in the melting zone. The dripping hot metal also utilises carbon, both for carburisation of the iron as well as for the direct reduction reactions, so below the melting zone where coke is consumed additional voidage is created. A substantial part of the voidage is created in the melting zone, and this implies that the flow of material is concentrated to the "ring" where the highest amount of ore is charged into the furnace. Therefore, at low coke rates, a high local radial concentration of ore in the circumference, notably at the wall area, has to be avoided.

The burden descent is sometimes characterised by irregularities, e.g. hangings, where there is little or no burden descent due to internal bridges formed in the furnace due to material glueing together or due to fluidisation of flooding. Hangings are often followed by fast, uncontrolled burden descent, so-called slips, which are undesirable. Slips disrupt the layer structure within the furnace, and then the permeability for gas flow deteriorates. Poor burden descent arises majorly at the cohesive zone.

The descent of the burden is thus due to the gravitational force which exceeds the counteracting upward drag forces of the ascending gas. The latter is manifested as a pressure difference between the blast and top gas.

3 SEGREGATION IN BLAST FURNACE

Segregation introduces irregularities into the blast furnace which is undesirable. It is also unwanted because it reduces the void (which is available for gas flow) and the residence time of the particles, which is detrimental for the heat transfer and the reduction reactions. In addition to percolation, other interesting effects of the particles occur: When the ore-bearing material is charged into the furnace, it may push the coarse and lighter coke particles on the top of the coke layer towards the centre. This effect is termed the coke push. It is more pronounced when the furnace is on blast, and there is a sieving effect because of the impact force.

Nevertheless, the primary cause of segregation in the blast furnace is by percolation. Ketterhagen et al. (2008) listed various mechanisms through which segregation occurs and they are air current, trajectory, rolling, the angle of repose, sieving, push away impact, embedding, displacement, percolation, fluidisation, agglomeration and displacement driven by concentration. They summarised the 13 segregation mechanisms into four main categories, listed in the following. Percolation or sifting segregation: this occurs when there is a net movement of smaller particles through a matrix of larger particles in the direction of gravitational acceleration, and that is enhanced by local strain. Angle of repose: a material with a smaller angle of repose flow over a material of larger angle of repose, during, for example, heap formation in the filling of a bin. Trajectory segregation: this is observed when friction effectively reduces the velocities of smaller or more angular material moving down a chute which results in different trajectories upon discharge from the chute. Fluidisation or elutriation segregation: differences in drag forces on particles in a mixture will tend to fluidise or entrain the fine and/or light particles causing them to segregate.

Guha et al. (2009) studied particle size segregation in the falling stream of burden materials using a bell-less top set up in a blast furnace. It was found for all the three types of burden materials, i.e., lump ore, sinter and coke, that there was a tendency of size segregation into two or three size fractions. Larger-size particles have a distinct tendency to segregate towards the outer part of the stream, and the smaller size particles segregate towards the inner part of the stream, whereas the intermediate-size particles distribute across the falling stream. This tendency of size segregation in the falling stream of burden appears to be enhanced at higher

chute angles. The particle size distribution in the feed burden material also affects the segregation behaviour to a large extent.

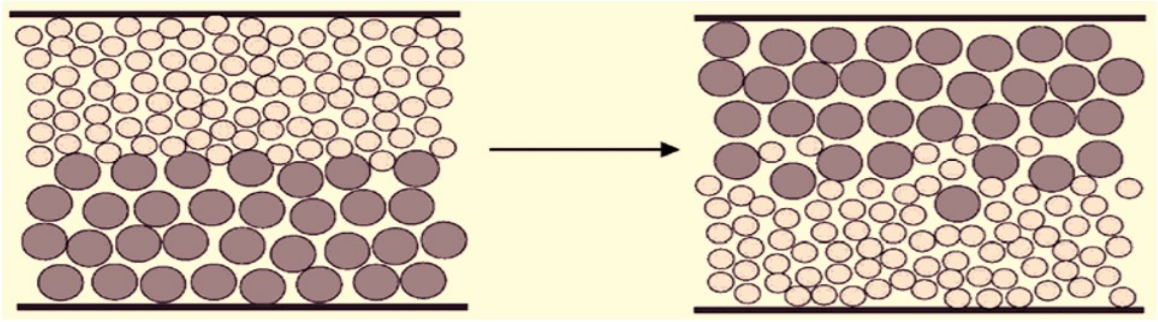

Figure 5: The percolation phenomenon (Hashim et al., 2008)

3.1 Percolation Parameters

Tang and Puri (2005) defined percolation as the movement of small particles through a large particle bed with external energy input. The movement of the percolating material within a parked material could be in the vertical direction or the horizontal direction, which is then quantified by percolation velocity and the radial distribution function. For a single percolating particle, the percolating velocity has been found to be constant both computationally (Rahman et al., 2008, Remond, 2010) and experimentally (Bridgwater and Ingram, 1971). This was also concluded from the results of this thesis.

The residence time distribution of particles represents the time it takes for them to pass through the system. The percolation velocity is the average distance the material travels vs. the time taken, which can easily be obtained from the slope of the distance vs. time curve.

The radial distribution function is the probability distribution of finding the centre of a particle in a given position at distance r from a reference one,

$$\frac{r^2}{4E_r t} = \ln \frac{N_o}{N_o - N} \,, \tag{1}$$

where E_r is the radial dispersion coefficient, N_0 is the total number of the percolating particles, and N is the number of percolating particles having centres within radius r at time t

Coordination number is the mean number of particles touching a given one, i.e. number of contact points between a particle and its neighbours.

Segregation rate is the number of small materials that have percolated into the parking material divided by the time.

Percolation mechanisms have been studied by a simple shear apparatus developed for testing soils (Bridgwater and Ingram 1971, Scott and Bridgwater, 1975, Bridgwater et al., 1978, Johanson et al., 2005).

Tang and Puri (2005) summarised some qualitative features of percolation segregation:

PERCOLATION SEGREGATION: It always occurs under static conditions. It is prevalent in unit operations that require handling of granular materials. Percolation segregation occurs due to small movements of the coarse particle bed such as vibration, strain, swaying, shearing and shifting due to forces, especially gravity, and little contribution from Vander Waals and electrostatic force.

Because of the burden descent and increasing diameter of the stack region in the blast furnace, the burden experiences a strain. Small distortions in the coarse particle structure then occur. The small distortions cause fine particles to pass through the void created between the coarse particles. Because of percolation, the iron layer will become leaner of fine particles and the coke will be enriched with the iron particles.

SIFTING is a form of top-down segregation were small particles are entrained and flow through the interstices of the coarse particle matrix. It is similar to percolation with the difference that sieving occurs in a dynamic condition like surface flow while percolation occurs in static bed conditions. In the blast furnace, sieving is carried out prior to charging the raw materials to reduce the number of fines in the system, but some fines are generated internally (by particle breaking, particle shrinking and gasification, etc.), so the occurrence of fines cannot be avoided. Furthermore, some burden materials, like pellets, are much smaller than other materials (e.g., coke), which makes pellet sifting possible. Sifting can occur in a material with broad particle size distribution when filling onto heaps. It results in a surplus of fine particles at the filling

point. Avalanches which induce shear deformation could also occur, allowing the smaller particle to sift through the open interstices by the larger coarser

Mio et al. (2009) enumerated some possible places at and in the blast furnace where segregation occurs. It could be at the top of the blast furnace as well as at the surge hopper, the conveyor, the bunker and the chute. Other potential places in which segregation occurs in a blast furnace include, but are not limited to, filling and emptying of the storage silo, and in skips due to vibration on the conveyor belt. The raw material storage bin is fed from a single opening, which could lead to the formation of a heap, which further enhances segregation. It also occurs during burden descent, which is the main focus of this thesis. Factors such as particle size distribution, feed rate, feed angle and other material properties also contribute to enhanced segregation.

Since iron-bearing components (ore, sinter, pellets) and coke are fed to separate storage bin, the material properties are similar, so mainly the size difference influences segregation in the storage bin.

In their study of percolation, Bridgewater and Ingram (1971) as well as Scott and Bridgwater (1975) found that from the geometry of close-packed spheres, the small sphere was able to percolate spontaneously due to gravity only if the size ratio $d/D < 0.1547$.

Bridgwater (1994) observed that the percolation velocity increases with an increase in size ratio and solids fractions, and goes to zero as the coefficient of restitution becomes one.

In their review, Hashim et al. (2008) explained the major parameters that affect percolation, which are provided in Table 1.

Table 1: Parameters controlling percolation rate

Description	**Comment**
Particle diameter ratio	Largest effect compared to other controlling parameters
Rate of strain	Percolation rates are faster below 0.4 s^{-1}
Normal stress	An increase in the normal stress reduces the percolation velocity
Particle density	Higher density particles percolate faster than lower density particles
Material properties	Particles with low elastic modulus percolate faster than those with a higher elastic modulus
Surface properties	Particles with smooth and shiny surfaces percolate faster than rough and scratched ones
Shape properties	Rounded shape percolate faster than an angular shape
Wall effects	Smaller particles percolated more rapidly at the wall than in the bulk

3.2 Ways to Reduce Segregation

Matsuhashi et al. (2012) found that coke-mixed charging improves the void fraction accompanying softening and shrinkage of the ore, and mixing of ore and coke at equal volumes can reduce the gas pressure drop by approximately 20% in comparison with single ore charging. This is mainly due to changes in the cohesive zone.

From results obtained by Windows-Yule and Parker (2015), the authors showed that transition from a binary to a ternary system does not change the underlying segregation mechanisms of distinct particle species, implying that findings from segregation studies of bidisperse systems could be extended to provide explanations and predictions of the behaviours of ternary systems.

Moreover, for the range of parameters explored, segregation due to differences in particle elasticity was found negligible.

It has been shown in the present thesis, and confirmed by some other work including, but not limited to, Tang and Puri (2004), that size ratio had the most significant contribution to percolation. Hence, to suppress percolation in the blast furnace, there is a need to reduce the size ratio between the iron pellet, sinter and coke to the smallest that could be technically achieved and is economical. Narrowing of the size distribution of feed material either by size reduction or size enlargement would also reduce the effect of percolation. Preventing heap formation or reducing the heap size and free-fall height under filling, in both silo and furnace, and with the use of various types of inserts and distributors in silos could also help.

In order to ensure that material is well mixed and composition uniformity is not substantially altered during discharging of silos, there is a need to ensure a constant fill and emptying height. Engblom et al. (2012) observed that side-to-side segregation was not entirely corrected for by introducing a hopper section in the silo designed for mass flow when segregation occurs at the levels of fill that are discharged last. From experimental results, Johanson (2014) found that segregation became conspicuous for material in the bin, in the last 11% of the emptying cycle. There was a need to avoid getting below 30% of the filling height. From the simulation result of Ketterhagen et al. (2009) for different hopper angles, it could be concluded that the segregation was minimal up to around 50% of fractional discharge and was considerable after 80% of the material had been discharged. Another recommendation would be to introduce a hopper at the bottom of the silo that induces mass flow.

4 THEORETICAL DEVELOPMENT

4.1 DEM

A simple search of the phrase “discrete element method” on the internet will turn up a mirage of published works on this technique. Originally created by Cundall and Strack (1979), the method has enjoyed the benefit of continual improvement over the years and it has already been extensively applied to simulate different granular flows in the industries, including process units such as drum mixer, blast furnaces, chute flows, bin and hopper charging and discharging flows (Chou et al. 2009, Li et al. 2008, Nguyen et al. 2009). It has been reported that DEM results are qualitatively in good agreement with results from experiments (Yu and Saxén, 2014) and has become a feasible numerical method for analysing discontinuous media. Although DEM has the advantage of being conceptually easy to grasp, a minus is that it is computationally demanding for large systems. The number of particles involved in a real industrial system could be over billions, where each particle’s motion, interaction with other particles or boundaries are computationally tracked. This poses challenges in the application of the discrete element method and makes the simulation of many industrial processes still unfeasible.

Various methods have been developed to reduce the computational time by enabling simpler calculation, e.g. using lower Young modulus, mono-sized particles, multi-sphere particles, optimising hardware parallel computing and developing more efficient DEM algorithms.

4.2 Governing Equations and Force Models

Rotation and translation are the two possible types of motion that particles in granular flow experience. During motion the particle interacts with the surrounding fluid, neighbouring particles, or walls through which the momentum and energy are transferred. However, the individual particle motion is not only affected by the forces and torques originating from its immediate neighbouring particles and vicinal fluid, but also through the propagation of disturbance waves by particles and fluids far away. The complexity of such a process has defied any attempt to model this problem analytically.

In DEM, the numerical time step that is utilised should be less than a critical value that enables the assumption that, during a single time step, the resultant forces on a particle could be determined entirely from its interaction with the contacting particles and vicinal fluid for a particulate system. In addition, it is assumed that disturbances cannot propagate from the particle and fluid farther than to its immediate neighbouring particles, and vicinal fluid is valid (Cundall and Strack, 1979). The time step has to be small enough to enable granular system stability and large enough to keep the computational workload reasonable.

The Rayleigh time step is the time required for the shear wave to propagate through a solid particle. It can also be defined as the theoretical maximum time step for a DEM simulation of the quasi-static particulate collection, in which the coordination number (total number of collision per particle) for each particle remains above 1. The Rayleigh time is given by

$$T_R = \frac{\pi R \left(\frac{\rho}{G}\right)^{\frac{1}{2}}}{0.1631v + 0.8766}, \tag{2}$$

where R is the particle's radius, ρ the density, G the shear modulus and v the Poisson's ratio. The formula assumes that relative velocity between contacting particles is very small. In the simulation to be presented, the coordination is high so, the maximum fraction of the Rayleigh time step used was 20%. The time integration used for all simulation was the Euler method, which when given the initial boundary condition, is used to calculate the state of the system such as forces, positions at a subsequent time from the state of the system at present for first order and first degree differential equation.

For a particulate system with a large number of fine particles, non-contact forces such as the van der Waals and electrostatic forces are usually included. Armed with this knowledge, Newton's second law of motion can then be utilised to describe the motion of individual particles.

With reference to the notation in Figure 6, the governing equations for the translational and rotational motion of particle i with mass m_i and moment of inertia I_i are

$$m_i \frac{dv_i}{dt} = \sum_j F_{ij}^c + \sum_k F_{ik}^{nc} + F_i^f + F_i^g \quad (3)$$

$$I_i \frac{d\omega_i}{dt} = \sum_j M_{ij}, \quad (4)$$

where M_{ij} and F_{ij}^c are the rotational torque and contact force acting on particle i by neighbouring particle j or walls, F_{ik}^{nc} is the non-contact force acting on particle i by particle k or other sources, F_i^f is the fluid– particle interaction force on particle i, and F_i^g is the gravitational force, while ω_i and v_i are the angular and translational velocities of particle i, respectively.

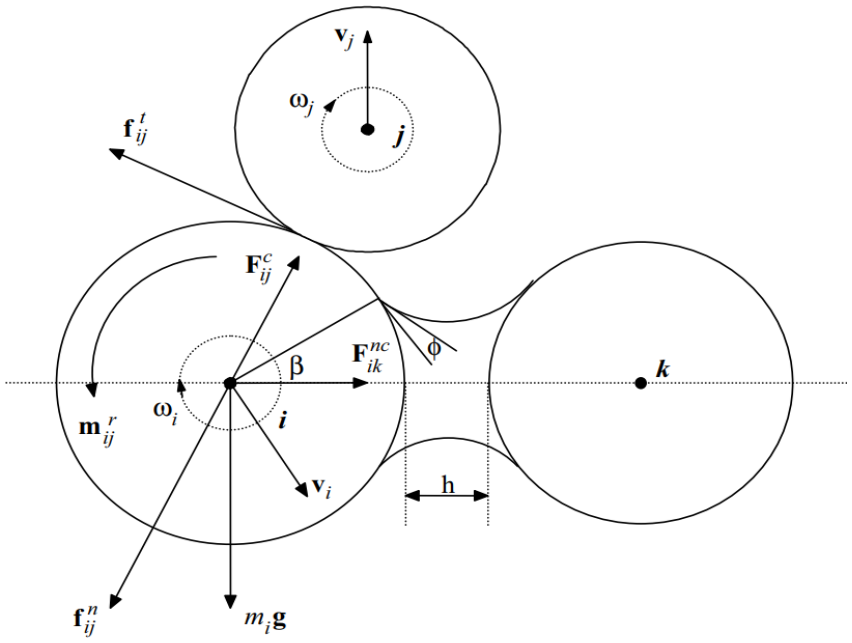

Figure 6: Schematic of forces and torques considered in DEM

Various models have been developed over the years in order to express and calculate these forces and torques, which will be discussed below. Once the forces and torques are known, Eqs. (2) and (3) can be readily solved numerically. Thus, the trajectories, velocities and the transient forces of all particles in a system considered can be determined.

The interparticle forces act at the contact point between particles, which is not a single point but on a finite area due to the deformation of the particles rather than the centre of mass of the particle, and they will generate a torque causing the particle to translate and rotate.

In reality, the shapes of the individual particle in the granular material are not spherical, which complicates the determination and calculation of contact points and forces (Zhu et al., 2007; Zhu et al., 2008). Techniques that have been developed to tackle this challenge include modelling the non-spherical particle as a collection of spherical particles (Bertrand et al, 2005). This approach, where multiple spheres are locked ("clumped") to each other, is flexible. It can be used to handle particles of very complex sizes and shapes, with the advantage that only the contact model for a spherical particle is used. On the downside, its accuracy is reduced, and it

increases the number of spheres in the system significantly, which usually increases the calculation time substantially. Another technique considered is based on particles of other but given shape, for example, cylinders, ellipsoids, and polygons, and determines whether or not there is a contact between two such neighbouring particles by solving the underlying mathematical equations (Dziugys and Peters, 2001; Langston et al., 2004). In this thesis, a soft contact approach is adopted which allows for deformation during a collision. The contact force model used is the Hertz-Mindlin non-linear spring-dashpot while the particle was modelled as a collection of spherical particles.

4.3 Hertz-Mindlin (No Slip)

Due to its efficient force, calculation and high accuracy, the Hertz-Mindlin contact model is the default model used in EDEM® - a commercial computational tool utilised in this work which can be used for the simulation, visualisation and analysis of particle flow. In this model, the normal force and tangential force model are based on Hertzian contact theory and the work by Mindlin and Deresiewicz. Both tangential and normal forces have damping components, where the damping coefficient is a function of the coefficient of restitution. The tangential friction force follows the Coulomb law of friction model, while the rolling friction is implemented as the contact independent directional constant torque model.

The normal force, F_n, is related to the normal overlap δ_n by

$$F_n = \frac{4}{3} E^* \sqrt{R^*}\, {\delta_n}^{\frac{3}{2}}. \tag{5}$$

The equivalent Young's Modulus $E^*$and the equivalent radius R^* are expressed respectively as

$$\frac{1}{E^*} = \frac{(1 - v_i^2)}{E_i} + \frac{(1 - v_j^2)}{E_j} \tag{6}$$

$$\frac{1}{R^*} = \frac{1}{R_i} + \frac{1}{R_j}, \tag{7}$$

where R_i, E_i, V_i are the radius, Young's Modulus, and the Poisson ratio if sphere i, while symbols with subscript j the corresponding variables for sphere j. Additionally, there is a damping force, F_n^d given by

$$F_n^d = -2\sqrt{\frac{5}{6}}\,\beta\sqrt{S_n m^* V_n^{rel}}\,, \tag{8}$$

where $m^* = (\frac{1}{m_i} + \frac{1}{m_j})^{-1}$, is the equivalent mass, V_n^{rel} is the normal component of the relative velocity. The variables, β and S_n (the normal stiffness), are given by

$$\beta = \frac{\ln e}{\sqrt{ln^2 e + \pi^2}} \tag{9}$$

$$S_n = 2E^*\sqrt{R^*\delta_n}\,, \tag{10}$$

where e is the coefficient of restitution. The tangential force, F_t, depends on the tangential overlap δ_t

$$F_t = -S_t\delta_t\,, \tag{11}$$

with tangential stiffness given by

$$S_t = 8\ G^*\sqrt{R^*\delta_n}\,, \tag{12}$$

Here, G^* is the equivalent shear modulus. Additionally, the tangential damping is given by

$$F_t^d = -2\sqrt{\frac{5}{6}}\,\beta\sqrt{S_t m^* V_t^{rel}}\,, \tag{13}$$

where V_t^{rel} is the relative tangential velocity. The tangential force is limited by Coulomb friction $\mu_s F_n$, where μ_s is the coefficient of static friction.

For simulations in which rolling friction is important, this is accounted for by applying a torque to the contacting surfaces.

$$\tau_i = \mu_r F_n R_i \omega_i \,, \tag{14}$$

where μ_r is the coefficient of rolling friction, R_i the distance of the contact point from the centre of mass and ω_i , the unit angular velocity vector of the object at the contact point.

5 MATERIAL AND METHOD

5.1 Cases Studied In This Thesis

This section gives a general overview of the computational studies carried out in this thesis. One may categorise the tasks into two cases, with further sub-classification with focus on studying intraparticle percolation. The cases are illustrated in Figure 7 and the geometries in Figure 8.

Case 1: BF-like setup

This case studies the percolation of smaller particles (pellets) into an underlying layer of larger particles (coke). The problem thus emulates part of the conditions in the upper part of the blast furnace, where layers of ore and coke alternate. For the case of simplicity, however, the geometry is cylindrical (cf. top left panel of Figure 8). The case can be further classified into two subcases, which study the effect of particle interaction parameters and the effect of process parameters. In both systems, a layer pair of uniform thickness is created and descended in a domain.

In the first subcase, the effect on percolation of the coefficient of static and rolling friction of the pellets was studied, where a layer pair descends in a cylindrical domain.

In the second case, the effects of process conditions on percolation were studied. The size ratio between the particles, here expressed as the ratio of the mean diameter of coke and pellets, was analysed. The coke diameter was taken to follow a normal distribution, represented by discrete classes capped with upper and lower limits to prevent unreasonably large and small particles. Other important factor studied were the descent rate as well as the effect of pressure exerted on the descending layers, mimicking the weight of the overlaying burden material. Furthermore, the role of multiple layers was investigated with the purpose of analysing if the material kept the layered structure during descent.

The computational study was augmented by an analysis of the impact of an expansion in the domain, increasing the radius of the circular cross-section, yielding a conical geometry like the one in the BF shaft (Figure 8, top right subpanel).

Finally, as a related case, a small-scale experimental system with glass beads and small plastic particles studied in a recent B.Sc. thesis (Jansson, 2019) was briefly analysed by DEM. As the layers in this bed do not descend, i.e., the bed is stagnant, it was exerted to vibration to trigger percolation of the smaller plastic spheres. In this case study, all particles were spherical and the geometry cylindrical (Figure 8, top left subpanel).

Case 2: Pellet silo

A large raw material silo with intermittent charging and emptying was also studied, with the goal to analyse the behaviour of small particle fractions in the silo and its outlet at the bottom. The silo was operated a limited number of cycles to study dynamic effects. In the first subcase, a silo with a single opening was studied, while in a later case a somewhat larger silo with three holes was analysed (Figure 8, bottom left and right subpanel, respectively).

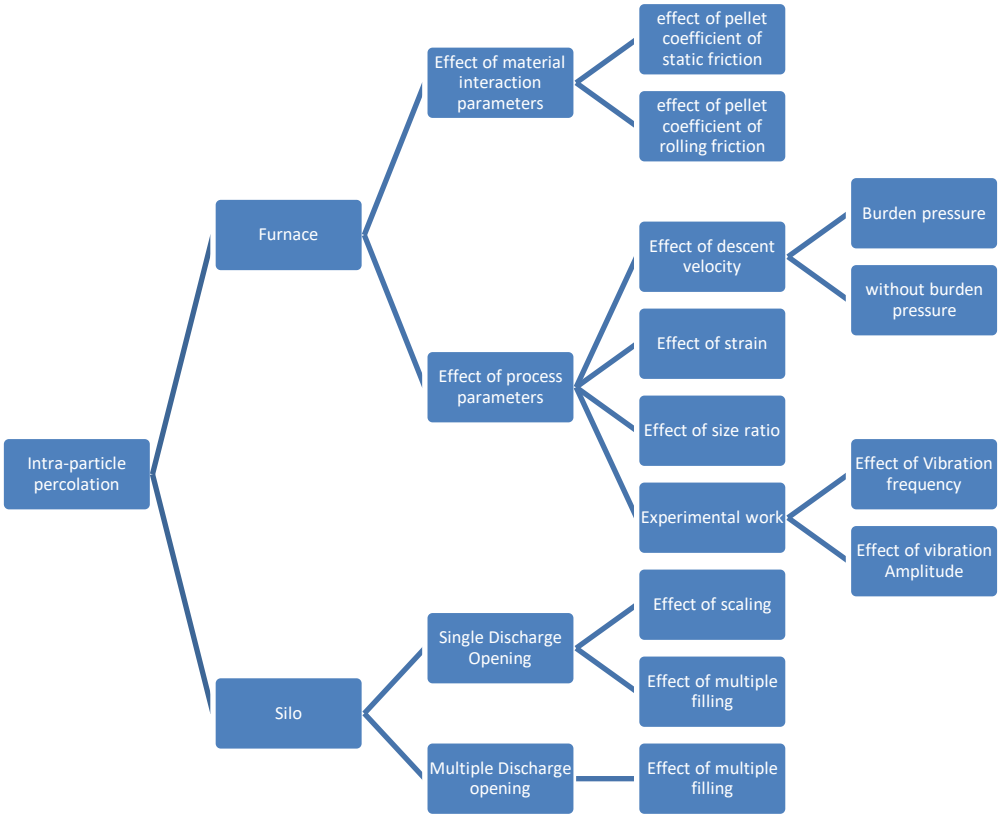

Figure 7: Graphical illustration of the cases studied in the thesis

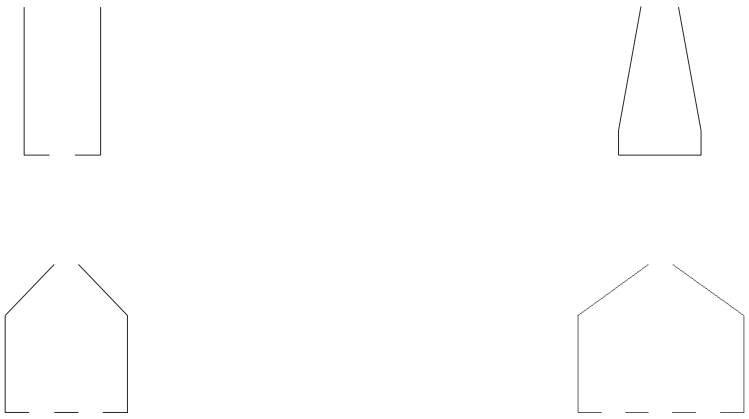

Figure 8: Schematic of cases studied: Top left: Cylindrical domain. Top right: Conical (shaft-like) domain. Bottom left: Silo with one opening. Bottom right: Silo with three openings.

5.2 Simulation Conditions

Discrete Element Method (DEM) simulations and analysis were conducted using EDEM® 2017 bulk material simulation software provided by DEM Solutions Ltd., Edinburgh, Scotland, UK. The particles used in the model are similar to those regularly used for the simulations of granular flow in process industries. They are non-cohesive, and the shapes are modelled as spheres (for pellets) or using the multi-sphere approach (for coke, as depicted in

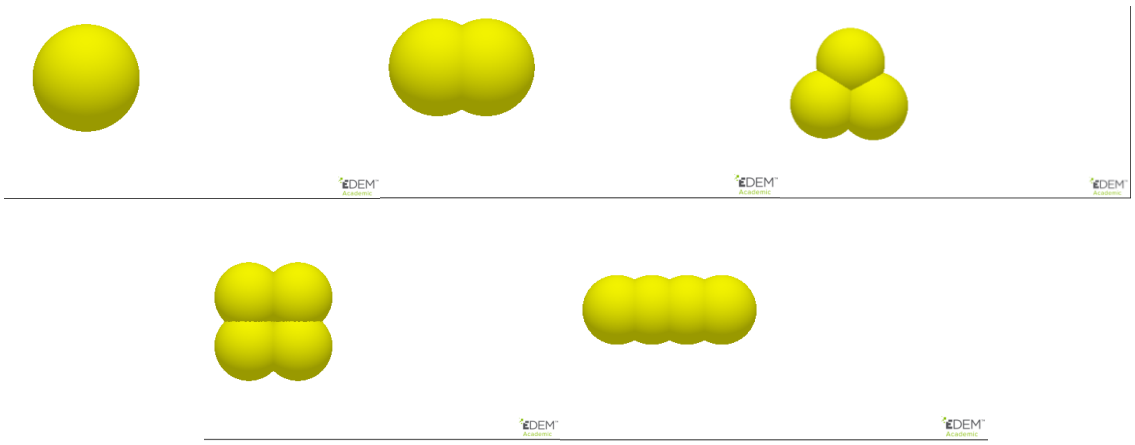

Figure 9). The simulations aim at closely mimicking the real process, but several simplifications must be introduced to make the solution of the problem feasible. The base parameters used for the simulation are listed in Table 2. For convenience, unless otherwise specified, the effect of any variable is considered with different numerical values, while other variables are fixed at fiducial value.

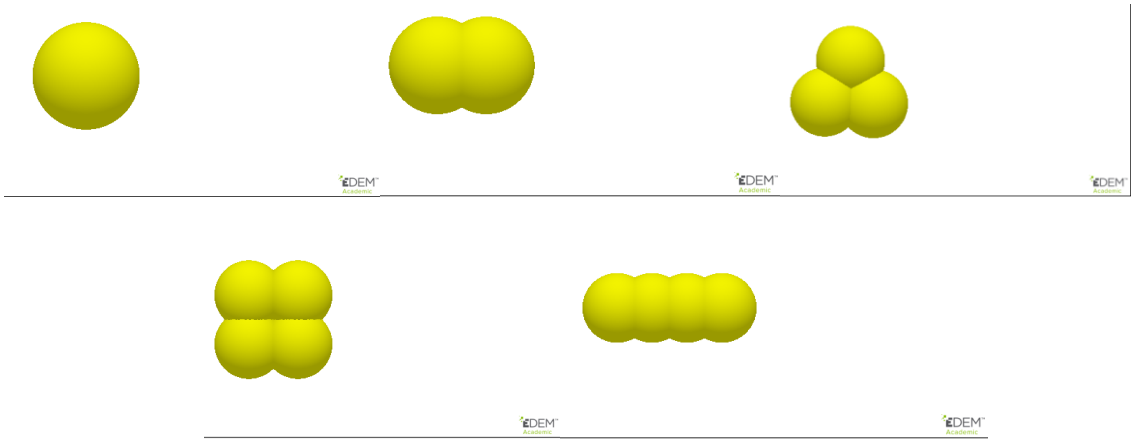

Figure 9: Particle shape representation in EDEM

The model geometry was created using CAD software and imported as .iges files into EDEM®. The iron pellet was assumed spherical while four different shapes for the coke material were used. The coke material size distribution is represented by the normal size distribution, while the average value is what is stated. In the simulations of the conditions in the blast furnace, the coke and iron pellets were generated in alternating layers and were afterwards allowed to descend by moving a bottom plate, upon which the lowest layer resided, at a constant velocity. In the case of the pellet bin simulations, a bed of pellet was first generated in the geometry, and then an opening was created at the bottom to allow for pellet discharge. After the first round of discharge is completed, new pellets are created and fed on the existing pellet bed.

In the simulations mainly the geometry was downscaled while keeping original values of the material interaction properties. An angle of repose test by Lommen et al. (2014) showed that a material stiffness reduction could be applied without altering the simulation results if the shear modulus is kept above 10^7 Pa or the average normal overlaps are kept below 0.3% of the particle radius. This change saves time in the simulations as larger time steps can be taken. Although

material properties could be determined in experiments or by calibration with DEM simulations from literature, the material properties used in the simulations of the present thesis were taken from Mitra (2016) and the EDEM® material database.

Table 2: Base material and interaction properties used in the simulations

Material	**Parameter**		**Value**
Ore	Diameter, mm		5
	Density, ρ (kg/m3)		4400
	Poisson's ratio, υ_P		0.25
	Shear Modulus, G_P(Pa)		10^7
	Coefficient of restitution	Ore	0.55
		Coke	0.5
		Wall	0.5
	Coefficient of static friction	Ore	0.04
		Coke	0.5
		Wall	1.0
	Coefficient of rolling friction	Ore	0.05
		Coke	0.01
		Wall	0.01
Coke	Diameter, mm		20
	Density, ρ (kg/m3)		1500
	Poisson's ratio, υ_P		0.25
	Shear Modulus, G_P(Pa)		1 e^{+7}
	Coefficient of restitution	Ore	0.5
		Coke	0.55
		Wall	0.5
	The coefficient of static friction	Ore	0.5

		Coke	0.92
		Wall	1
	The coefficient of rolling friction	Ore	0.05
		Coke	0.05
		Wall	0.15

In all the simulations presented, the coke particles size followed a normal distribution. The standard deviation was set to 5% of the mean size. In order to reduce the computation time, a size limit was imposed to eliminate particle sizes deviating more than 25% from the mean size. Large sizes are in practice sieved out, while small sizes increase the number of particle in the system and also prolong the computation time as they affect the largest feasible time step that can be taken.

The geometries were first created with a CAD software and then converted to .stl or .iges files which are the format accepted by EDEM. Simpler geometries were created directly with EDEM.

The contact model utilised in the simulations of this thesis is the famous Hertz-Mindlin no slip model, which was selected from the physics section of the software.

The values for gravitational acceleration and the domain/model boundary were inserted into the environment section. Sometimes the periodic boundaries condition were implemented in other to eliminate the wall effects.

In all of the simulations carried out, the Euler time integration method was utilised. The values reported in the literature for the percentage of the Rayleigh time step are usually between 20% and 40% to ensure stability. However, these were found infeasible for most of the cases treated here, so values between 1% and 20% of the Rayleigh time step were instead used. It slows down the simulation, because the simulator has to detect all possible contact at every time step, which is in order of microseconds.

Results obtained from Engblom (2012) and this thesis work showed that similar segregation patterns was obtained irrespective of the scale of the system aside from the magnitude of segregation.

The results data were exported to a data processor where different charts where obtained. The particles were coloured not just to improve aesthetic, but as trackers which enable easy identification of flow behaviour and pattern in the simulations.

Different slices were obtained from the geometries to enable internal visualisation of what happens inside the system which cannot be obtained in an experiment as the particles are opaque, which is one of the advantages of using the computational tools.

5.3 Simulation Procedure for Vibrating Bed

A system was studied consisting of a (transparent) Perspex pipe, into which a mixture of small and medium-sized glass beads was used to build an initial bed on a grid. On top of the gas bead bed, a layer of smaller particles was "charged", and the system was vibrated to trigger percolation of the small particles through the bead bed. The particles passing through the system were collected in a funnel and fed through a hose to a scales for weighing. The size of the geometry used in this simulation is the same as that used in the experiments undertaken in the work of Jansson (2019), where the system wall had an inner diameter of 14.4 cm and a height, including the bottom funnel, of 50 cm. The opening of the bottom sieve is 1.17 cm which was selected to allow for the passage of only the smallest particles. The bottom opening of the funnel had a diameter of 3 cm.

The number of large glass beads (d = 2.5 cm) was 65 while the number of medium-sized glass beads (d = 1.6 cm) used was 195, making the packed bed having a number ratio of 3:1 and size ratio 1.625:1. The estimated number of small particles used was calculated from the mass of the total number of particles divided by the mass of individual particles, yielding $739.6\ \text{g}/0.3\ \text{g} \approx 2470$. A vibration amplitude ranging from 0 cm to 1 cm was studied using a vibration frequency of 20 Hz. This shaking was considerably larger than in the experimental system to reduce the simulation time. In the figures to be presented, the small beads are yellow, medium glass beads magenta while the big glass beads are cyan.

In reality, there is a limit to the values of the variable stated above due to the size of the apparatus involved. From the simulation results, it could be seen that 20 Hz was the vibration frequency yielding the highest percolation, since increasing or decreasing the value decreased the percolation rate of the small glass beads. There was also not much difference observed in the percolation rate when the frequency was increased from 30 Hz to 50 Hz. The increasing vibration may have increased collision and bouncing which may, in turn, reduce the percolation rate due to energy dissipation. As for the effect of amplitude, the value 0.6 cm produced the highest percolation rate, but increasing the value above 0.4 cm had little impact on the percolation rate. It may be as a result of the larger and medium particle filling the void created by the strain experienced by the packed bed.

Table 3: Material and interaction properties used in the simulations of the experimental setup

Material	Parameter		Value
Glass beads	Diameter		25, 16, 6 mm
	Density		2500 kg/m^3
	Poisson's ratio		0.25
	Young's modulus		1e+07 pa
	Coefficient of restitution	Glass beads	0.005
		steel	0.005
	The coefficient of static friction	Glass beads	0.02
		steel	0.05
	The coefficient of rolling friction	Glass beads	0
		steel	0.01

6 RESULTS AND DISCUSSION

6.1 BF Shaft-Like Setup

6.1.1 Effect of Process Parameters

Error! Reference source not found.0 represents the case studied here, where two layers were built independently, then collapsed forming a layer pair and then descended with a velocity of 0.06 m/s. It is higher than the descent rate in the blast furnace, but was chosen to be slow enough not to create too strong dynamic effects, but fast enough to yield a reasonable computation time. The system is 50 cm high and has a square cross-section with side length of 30 cm. The total number of particles in the system was 8200, with 700 particles of coke (of different shapes, cf. Figure 9, and sizes) and 7500 iron pellet particles of uniform size.

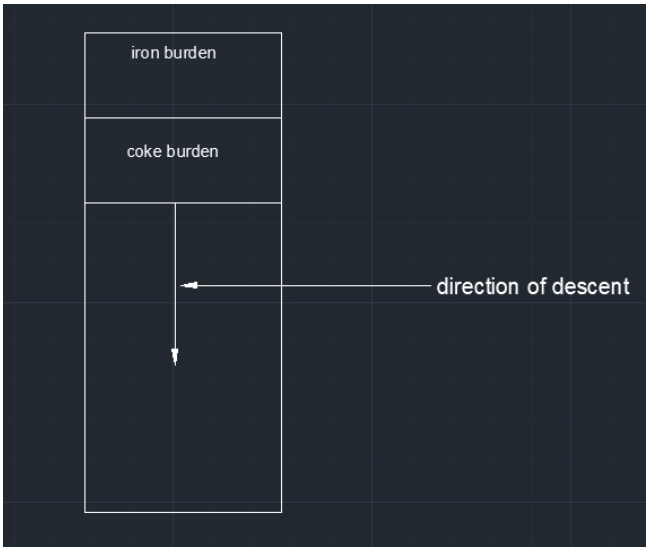

Figure 10: Setup for a system with a uniform cross section

6.1.1.1 Effect of Size Ratio

First, the effect of size ratio on percolation was studied. The size ratio is here defined as the ratio of average pellet diameter to the average coke diameter. The ratios studied were 1:2, 1:3,

1:4 and 1:5, where the pellets had a diameter of 5 mm. Virtual boxes are placed in the coke layer, as indicated in Figure 11.

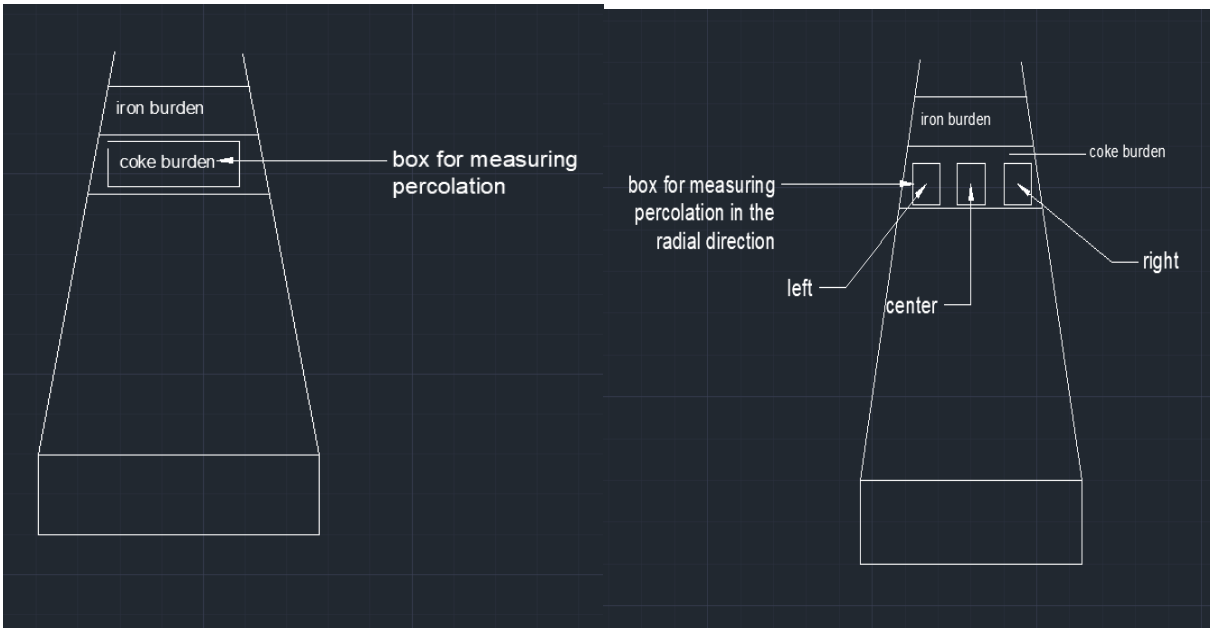

Figure 11: Virtual boxes placed in the coke layer to follow the percolation of pellets into it. Left: Overall percolation. Right: Percolation considering radial distribution.

Results are presented in Figures 12-14. Figure 12 shows a front view of the different stages of the bed during the computational experiment. The top panels show the layers just after complete particle generation and before the collapse, the middle panel just after the collapse (before the descent starts) and the bottom panel the bed material during descent. The size ratio in the figure is 1:4. During the first eight seconds, the burden particles were generated, during the time 8-15 s the pellet layer was collapsed on the coke layer to settle, while for the time 15-20 s the burden had a downward velocity. Percolation was quantified as the cumulative amount of pellet entering the virtual box (cf. left panel of Figure 11). Figure 13 shows the cumulative number of pellets that has percolated into the descending coke layer. It is seen that the initial collapse makes between 800 and 2600 pellets enter into the coke bed, strongly depending on the size ratio. It is mainly due to the percolation into the void of the top part of the coke layer. For the four runs, only one (corresponding to the size ratio 1:4) shows spontaneous percolation during the time the bed is stagnant, but also here the bed becomes static at $t = 12$ s. Next, the percolation

that is observed is induced by the descent of the bed. It is seen that a larger size ratio affects the response of the system, where a large ratio yields more immediate changes. The slope for all the size ratios, except 1:2, however, become very similar, and the highest size ratio eventually leads to a levelling out of the number of percolating particles. It may indicate that the bed is getting choked by the small particles.

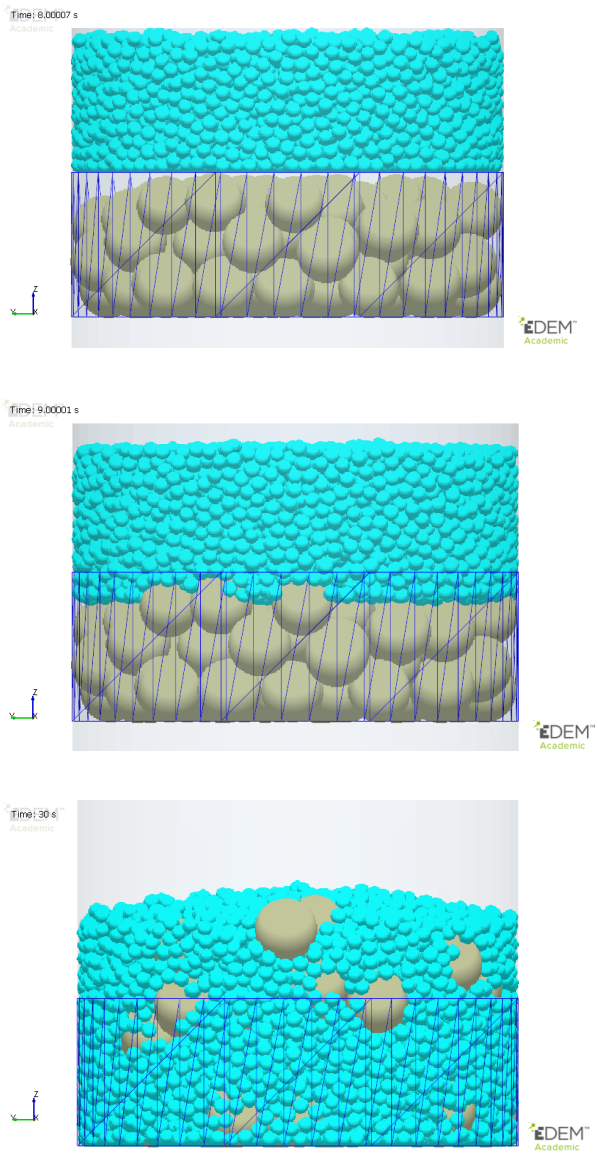

Figure 12: State of the two layers in the bed. Top: After generation. Middle: After collapse. Bottom: After the descent

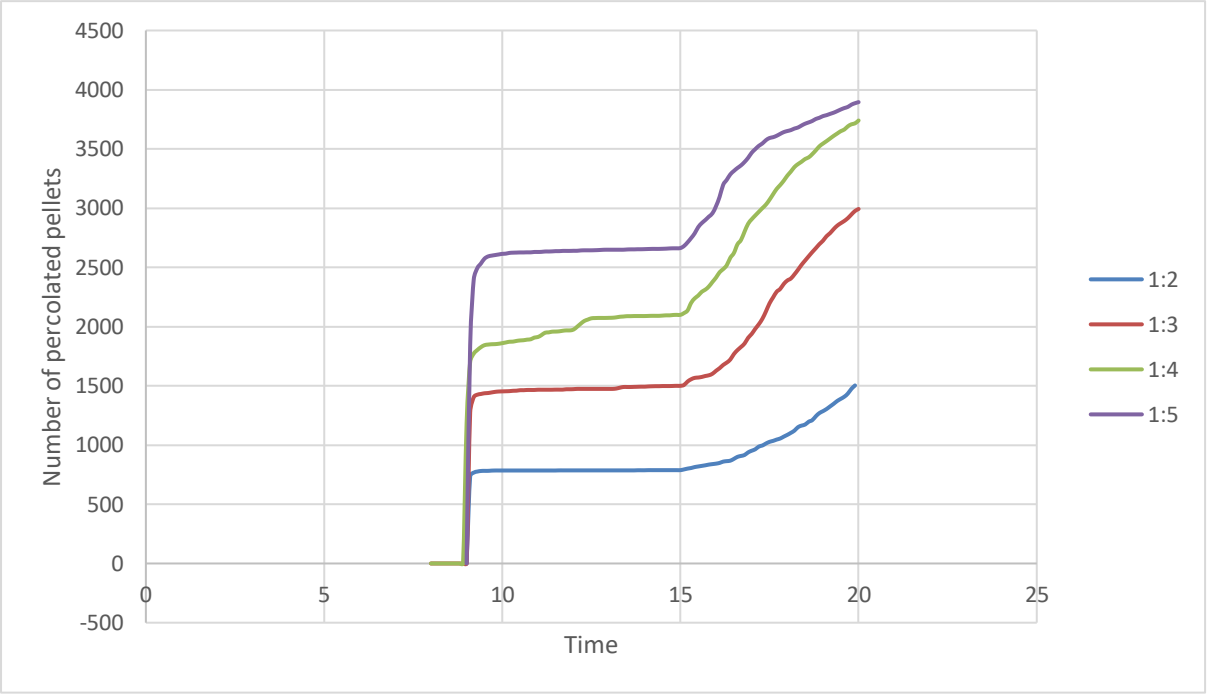

Figure 13: Cumulative number of percolating particles at different size ratio of pellets and coke

Figure 14 depicts the arithmetic mean of the particle velocity of the percolating material in the coke layer with time. The individual velocities are calculated by dividing the vertical component of the distance travelled by the time taken. The effect of particle size ratio on the average percolating velocity for the pellets is seen to be small as the velocity is relatively constant. These results agree with the observation by Rahman et al. (2008) for a single fine percolating particle type. However, the size ratio 1:2 shows different behaviour due to the very slow percolation rate as the layers start descending: This later leads to higher particle velocity.

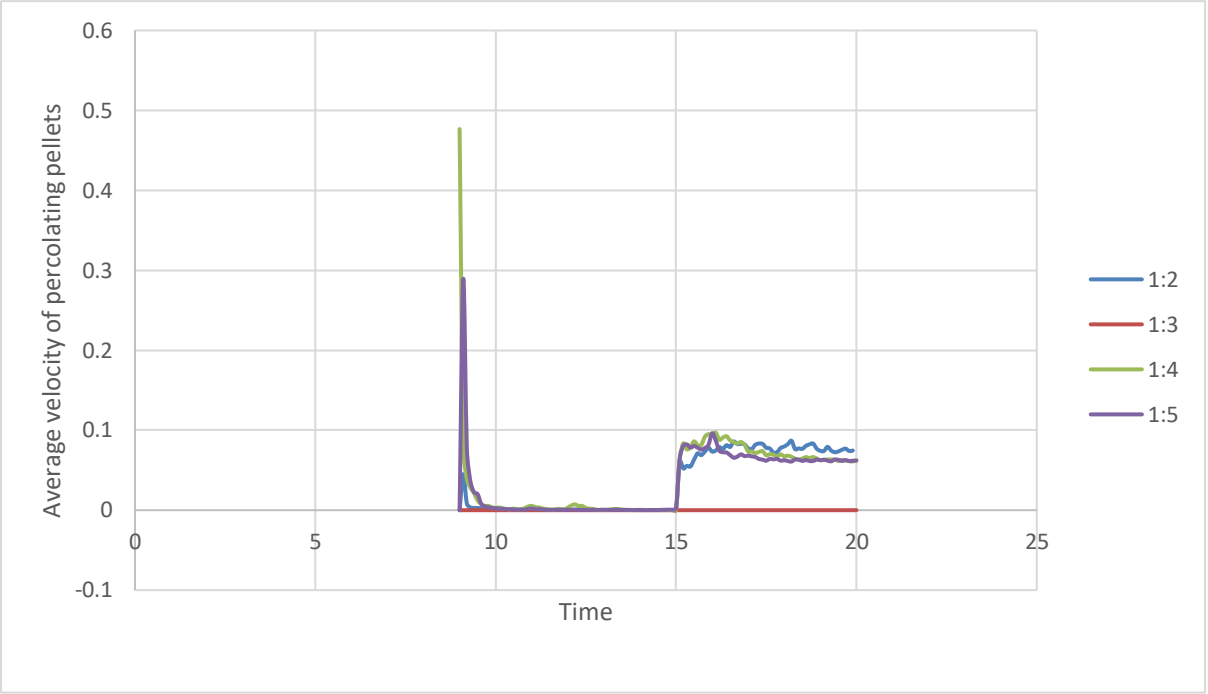

Figure 14: Average vertical component of the percolating pellet particles for different overall size ratios.

6.1.1.2 Effect of Descent Velocity

Next, the effect of descent velocity was studied for the size ratio of 1:4. In other respects, the experimental procedure was kept unchanged. The same bed formed after generation and collapse was used as the starting point before the descent to avoid stochastic effects in the layer formation process. The total number of percolating pellets in the coke layer is depicted in Figure 15, but at different descent rates,so also the residence time in the system varies: this explains why the experiments were ended in the time range 17.5-30 s. The segregation rate, which is reflected by the slopes of the curves, is seen to increase with the descent rate. A possible explanation for this is that a higher descent rate increases the bed voidage partly due to wall effects. The average descent velocities are presented in Figure 16.

In practice, it is difficult to control the descent velocity, as it is the result of voidage created due to the combustion/gasification of coke close to the tuyeres, melting of burden material, carburization of iron as well as the direct reduction reaction in the blast furnace. The overall descent rate naturally varies with the production rate, and the local descent rate may be higher at the wall due to the growing diameter of the shaft and this is studied later in the thesis.

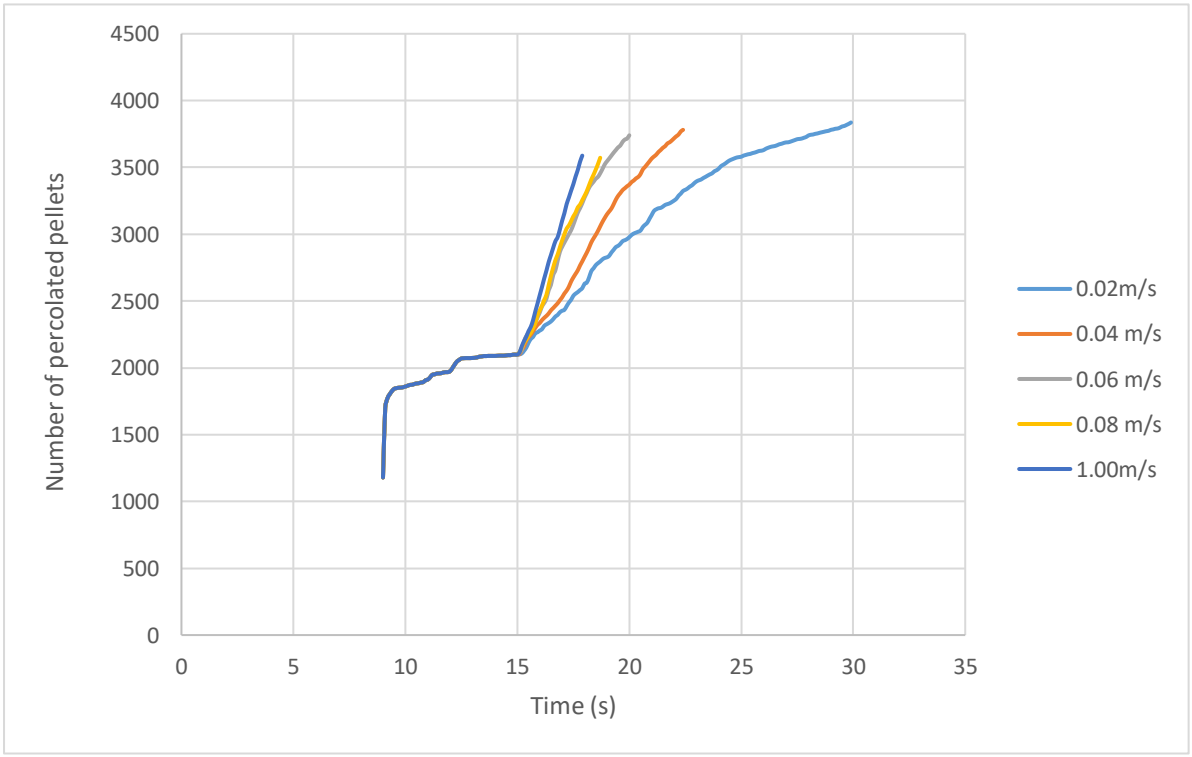

Figure 15: Cumulative number of percolated pellet particles at different bed descent velocities.

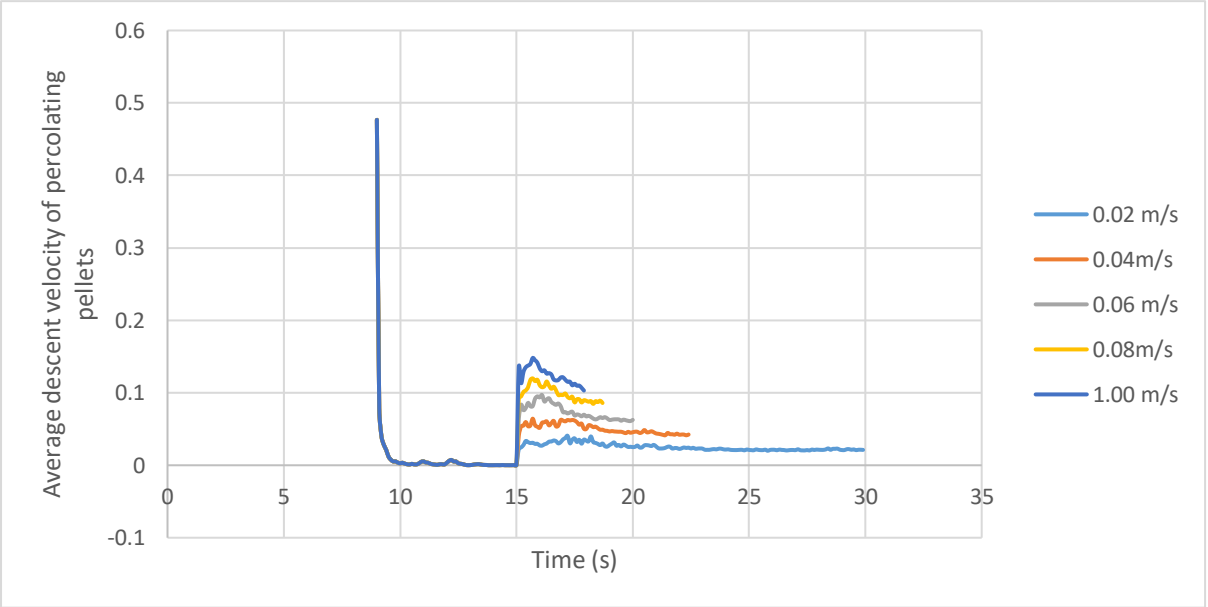

Figure 16: Average vertical component of the percolating pellet particles for different bed descent rates

6.1.1.3 Analysis of Radial Distribution

6.1.1.3.1 Effect of Size Ratio

The burden was computationally divided into three parts along the radial direction, named centre, left and right, as depicted in the right panel of Figure 11**Error! Reference source not found.**. The left and right virtual boxes are close to the wall, and symmetrically placed, where the wall effect would be experienced. Two different size ratios were considered here, 1:2 and 1:4. Like before, during the time 0-8 s, the burden material was generated, during the time 8-15 s the pellet layer was collapsed on the coke layer, while from 15 s onwards the burden was allowed to descend at the nominal speed (0.06 m/s). From Figures 17 and 18 one can see that the mass flow rate of percolating particles is higher at the centre than at the wall for both size ratios. (Note the different scale of the y-axis.) It is due to the 'wall effect'; friction at the wall causes particles (both coke and pellets) close to the wall to descend more slowly compared to the particles at the centre. The figures also show that the left and the right box receive an almost equal amount of pellets, as expected: the small differences are due to stochastic effects in the motion of the particles. Comparing the results for the two size ratios, one may note that for the case with the size ratio of 1:4 (Figure 18) the wall effect is seen to be less prominent. It is due

to the larger voidage created in the wall region due to the larger coke diameter, which makes the wall percolation stronger.

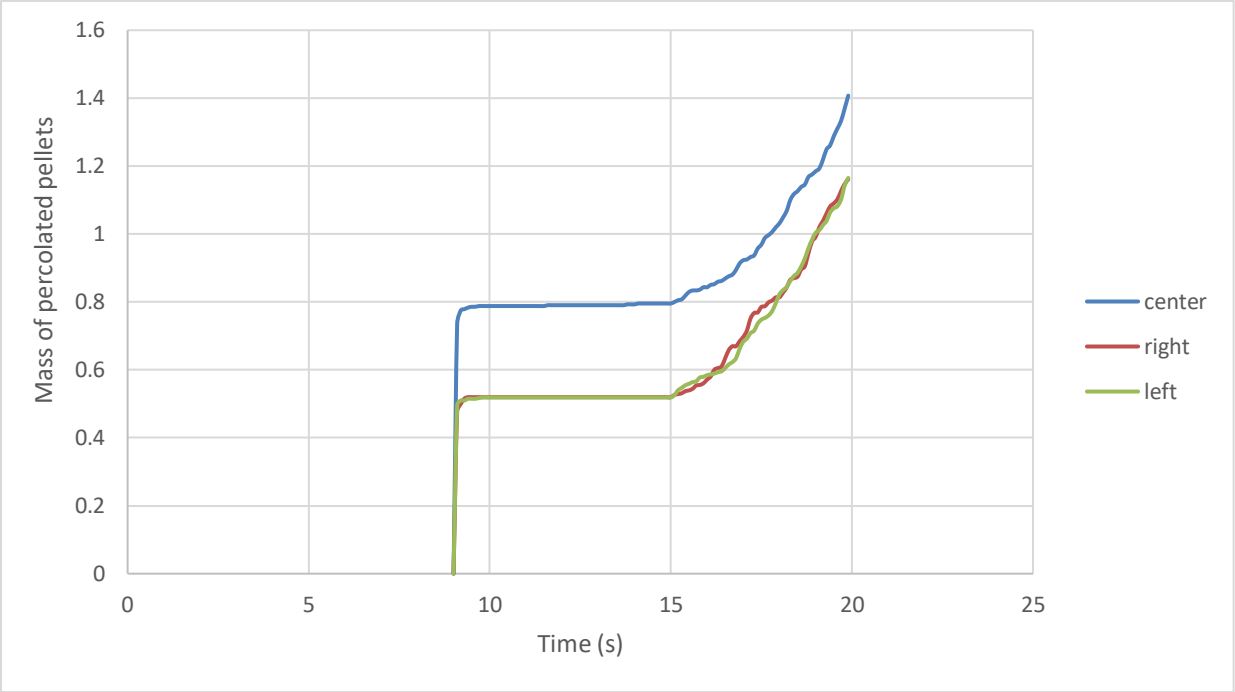

Figure 17: Mass of percolated pellet particles into the three virtual boxes depicted in the right panel of Figure 11 for a particle size ratio of 1:2.

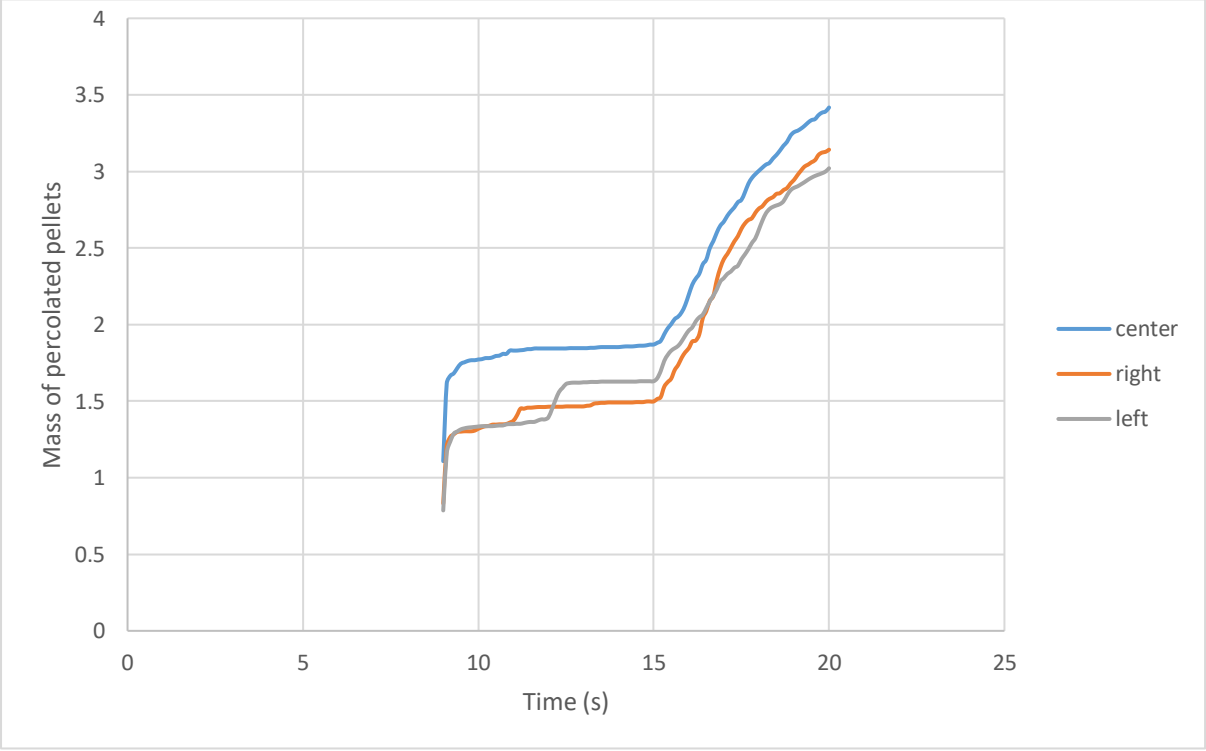

Figure 18: Mass of percolated pellet particles into the three virtual boxes depicted in the right panel of Figure 11 for a particle size ratio of 1:4.

6.1.1.3.2 Effect of Descent Velocity

Figure 19: Mass of percolated pellet particles into the three virtual boxes depicted in the right panel of Figure 11 for a particle size ratio of 1:4

illustrates the mass of percolated pellets vs. time with an emphasis on the segregation in the radial direction for the size ratio of 1:4 for a lower descent velocity, 0.02 m/s. The higher void is seen to make the differences in the radial direction less pronounced, and some asymmetry now occurs, since a large void increases the likelihood that local channels are formed. The percolation velocity for a size ratio of 1:4, but at two quite different descent velocities, 0.02 m/s and 0.06 m/s, are depicted in Figure 20. The average percolation velocity is seen to be rather constant in the radial direction, but the higher descent rate yielded a clearly higher percolation rate.

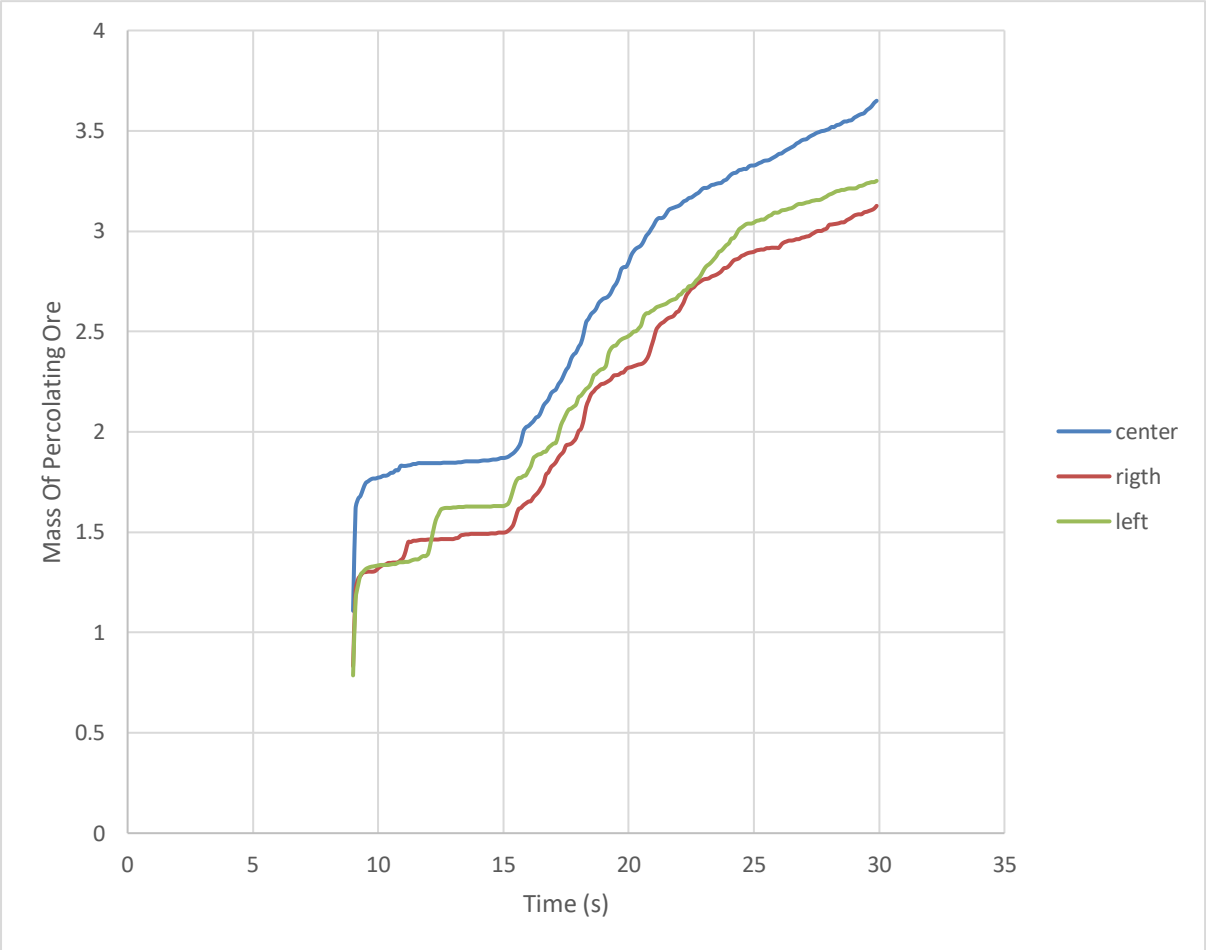

Figure 19: Mass of percolated pellet particles into the three virtual boxes depicted in the right panel of Figure 11 for a particle size ratio of 1:4

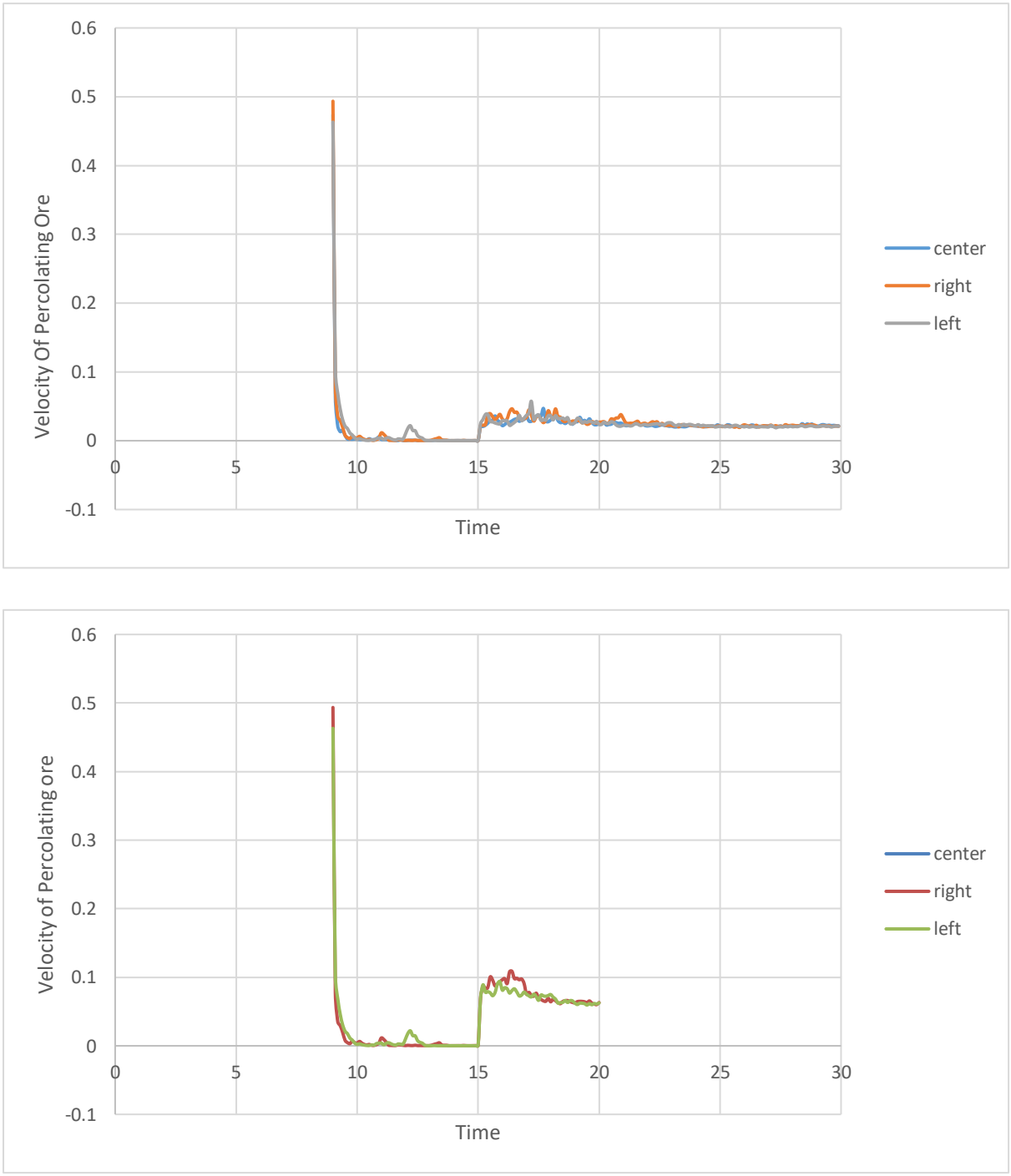

Figure 20: Average vertical component of the percolating pellet particles velocities at three radial positions for different bed descent rates. Top: 0.02 m/s. Bottom: 0.06 m/s

6.1.2 Effect of Material Interaction Parameters

6.1.2.1 Effect of Friction

Zhu et al. (2009) applied DEM to study the effect of particle properties on the percolation behaviour, including damping coefficients and sliding friction between the percolating and packing particles, diameter and density ratios of percolating to packing particles and Young's modulus of the percolating particles. They concluded that the damping coefficient and diameter ratio were the two dominant parameters that significantly affect the percolation. Decreasing the diameter ratio or increasing the damping coefficient would increase the percolation velocity and decrease the radial dispersion. Remond (2010) showed that the vertical and horizontal percolation velocities decrease with an increase in friction coefficient and small particle concentration, except for the mean vertical velocity at very low concentrations, as a result of the interactions of small particles with the packing been predominant as compared to interactions between small particles themselves. The influence of the friction coefficient is not noticeable for values of $\mu \geq 0.5$. Rahman et al. (2008) demonstrated that the percolation velocity increases while residence time increases with decreasing particle diameter ratio and coefficient of restitution. The effect of the packing height on the residence time and radial dispersion was eliminated when they were normalised by the average residence time and the product of the packing height and packing particle diameter.

In their work, Zhang et al. (2018) showed that the smallest particle scale mixing index appeared when the sliding friction coefficient was 1.0 and the rolling friction coefficient was $0.025(\frac{d_p}{\text{mm}})$. Moreover, a combination of a moderate rolling friction coefficient in a range of $0.01d_p$ to 0.1 d_p and sliding friction coefficient > 0.5 led to pronounced segregation. Asmar et al. (2002) showed that segregation increases with reduced friction, but increases with decreasing particle size ratio. For the system that Džiugys and Navakas (2009) studied, a higher rate of segregation intensity was obtained at low values of the dynamic friction coefficient, and it attained the minimum at $\mu_{\text{crit}} \approx 0.1$

6.1.2.2 The Effect of Coefficient of Static Friction

The effect of the coefficient of static friction (COF) of the ore particles was investigated for a burden descent rate of 0.06 m/s and a size ratio of 1:4. From Figure 21, which depicts the number of percolating ore particles vs. time, it can be seen that the friction coefficient plays a minor role: the trend remains similar for all cases studied, and the differences are merely stochastic. Also, Figure 22, which depicts the average percolating velocity, shows that the effect of the particle friction is negligible.

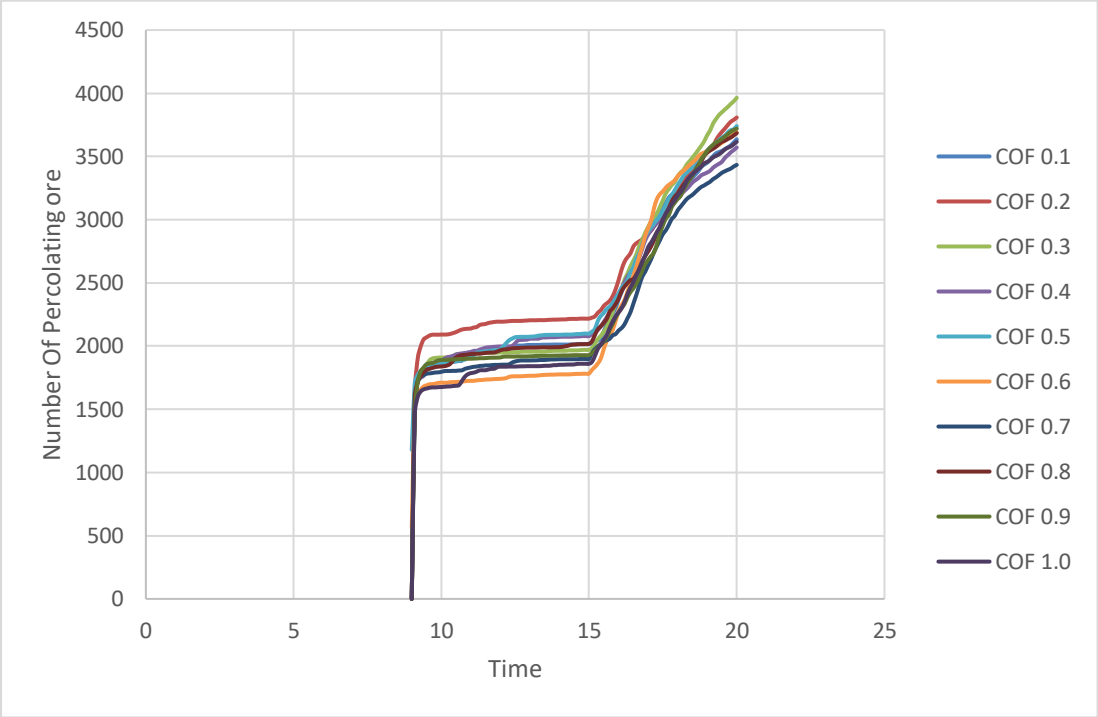

Figure 21: Cumulative number of percolated pellet particles for different values of the static coefficient of friction of the pellets

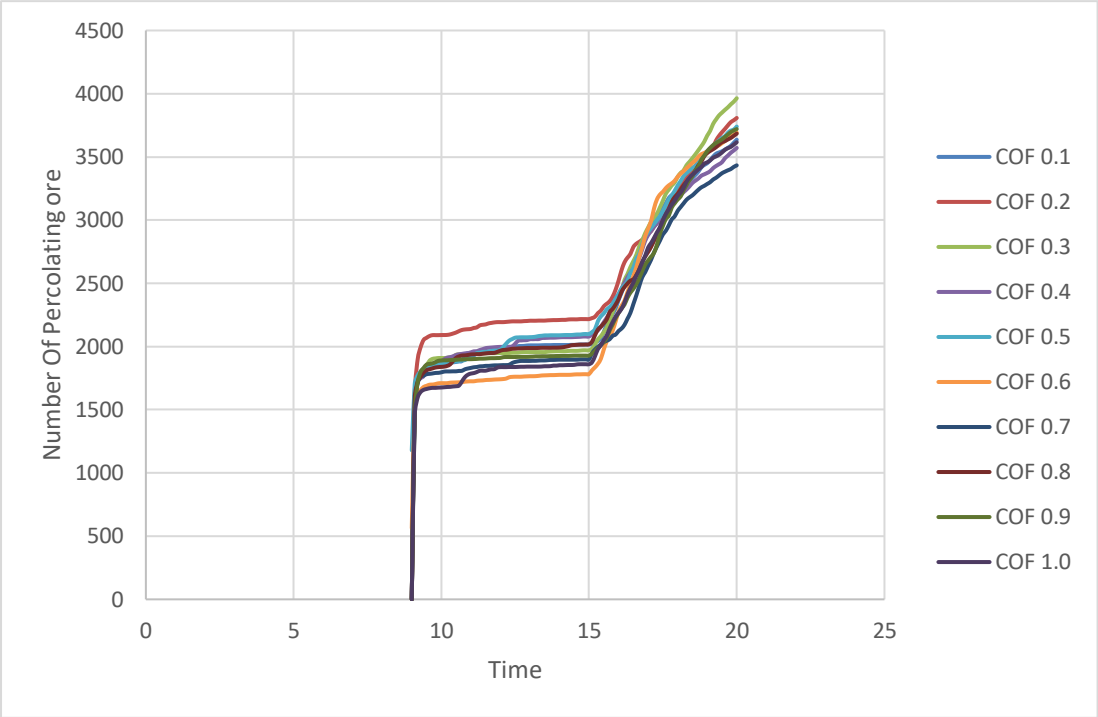

Figure 22: Average vertical component of the percolating pellet for different values of the static coefficient of friction of the pellets

6.2 Expansion of the Domain

The earlier studies were all conducted for a bed with a cylindrical diameter. However, the blast furnace shaft expands considerably from the throat region to the belly, making the layers spread out when they descend in the furnace. To study this effect, an expanding domain (cf. top right in Figure 8) was simulated to study the effect of strain on the percolation, i.e., the percolation that occurs when the burden materials move into regions with larger cross-sectional areas. The area was expanded by different shaft angles, where 90° means a shaft with vertical walls (i.e., cylindrical shaft, no expansion). In this system, the size ratio was 1:4 and the descent velocity of 0.06 m/s was applied. A throat diameter of 30 cm was used, just as in the cylindrical system. From Figure 23 it can be seen that decreasing the wall angle, i.e., increasing the expansion, considerably increases the percolation of pellets. For the cylindrical shaft, the number of percolated particles approaches 5000 at the end, while for the expanding shaft all pellets (about 40000) finally percolate, and the rate at which this happened (slope of the line) depends strongly on the shaft angle.

Even though the ratio between the diameters of the shaft and the particles is much smaller than in the real process, it may be concluded that the expansion of the shaft along with the descent of the burden is likely to yield a quite strong percolation in the regions close to the wall, where the increasing shaft diameter creates voids that the smaller and round pellets may percolate into. It is in line with the results found by Yu et al. (2011) in their experimental and computational study of a coke-pellet layer pair subjected to expansion.

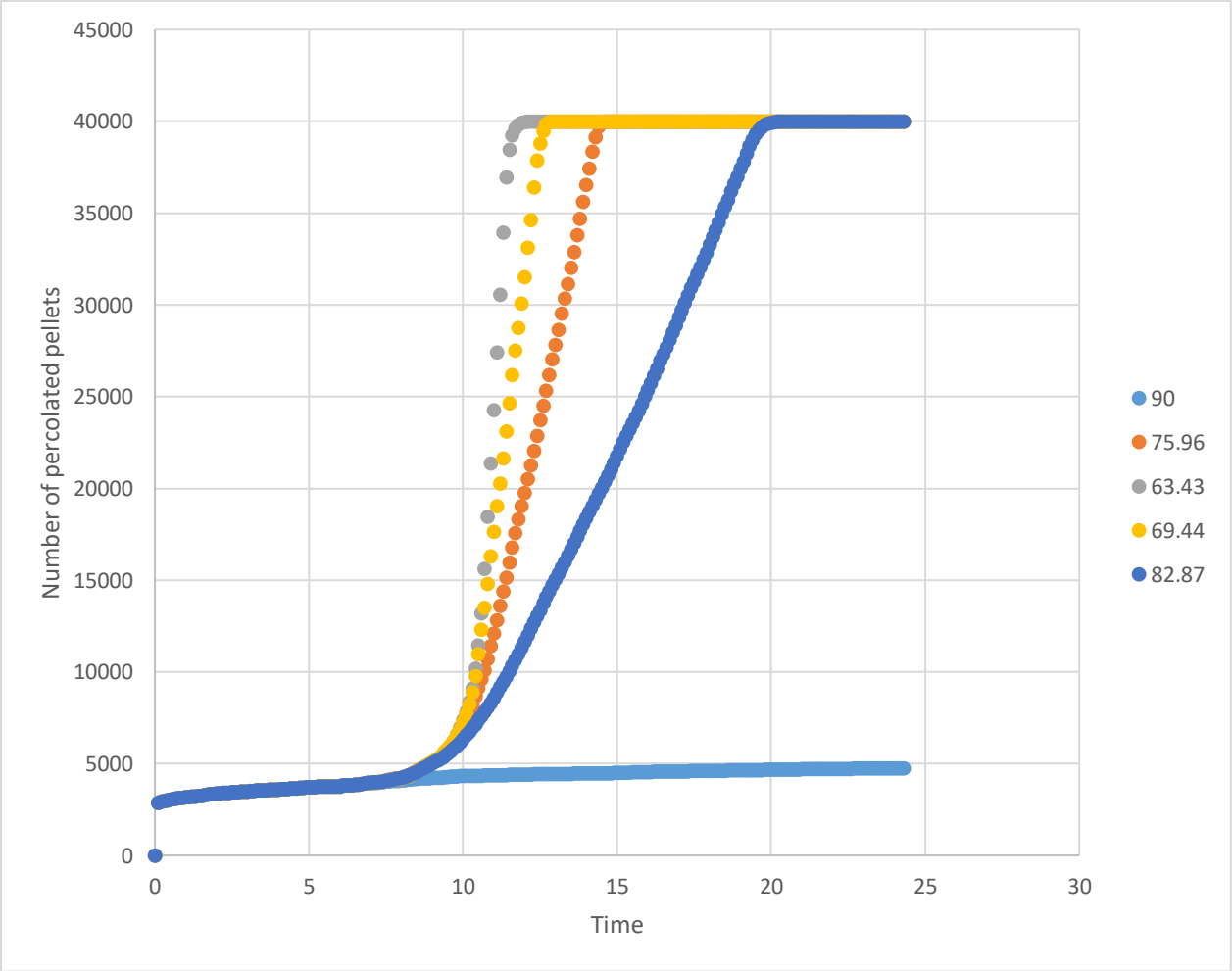

Figure 23: Cumulative number of percolated pellet particles for different angles of an expanding shaft (cf. top right panel of Figure 8).

It was observed that the layered structure was kept during the descent except deformation seen along the wall. Shaft diameter expansion increased the percolation and furthermore led to the formation of a clearly mixed layer at the wall, which would affect the voidage and consequently the gas distribution in the real system. Figure 24 shows (for the case with a size ratio 1:4 and a shaft angle 83°) front (left panel) and cross-sectional (right panel) views of the state of the layers at a point where the bed has descended about halfway through the expanding shaft. The wall effect is quite clear, leading to a U-shaped interface between the layers.

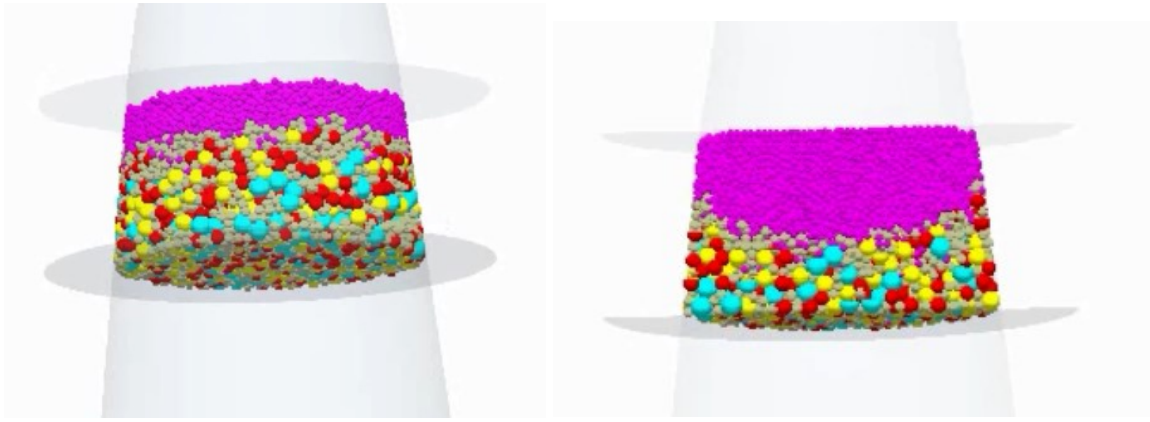

Figure 24: Front (left panel) and cross-sectional (right panel) view of the state of the layers at descending through the bed.

6.2.1 Effect of Pressure

All studies above focused on the percolation of smaller (pellet) particles into a bed of larger (coke) particles suffer from the drawback that they do not consider all main aspects of the full system. One such aspect is that the pressure of the overlying layers, which are not simulated in the present setup, may have an influence on the motion of the particles. Therefore, an attempt was made to consider the effect of the pressure of the burden column in the simulations.

A larger bed dimension was used here to make the findings more relevant from a practical point of view: the bed diameter was 0.5 m in the throat and 0.8 m at the belly, while the bed height was 1.8. The number of particles also increased, and are reported in Table 3.

The pressure was imposed by descending the lower surface of the system at a lower rate (0.06 m/s) than the upper (0.075 m/s) by putting a virtual plate on the pellet surface with the latter speed. However, the simulator seemed to move the "piston" in steps, which is why the pressure that initially was increased decayed with time, as seen in Figure 25. In an attempt to address this problem, another approach was made where an upper plate with a given descent speed was imposed, but more material was charged on top of it, which increased the simulated pressure on the layer pair. The increased pressure was found to increase the number of percolated particles, as seen in

Figure 26.

Figure 27 depicts the number of percolating for cases with different top pressure. It can be seen that increasing top pressure on the burden increases the extent of percolation.

Table 3: Number of particles used in the setup with pressure imposed on the layers.

Particle type	**Number**
Coke 1	3087
Coke 2	613
Coke 3	351
Coke 4	224
Pellet	58520
Total	62795

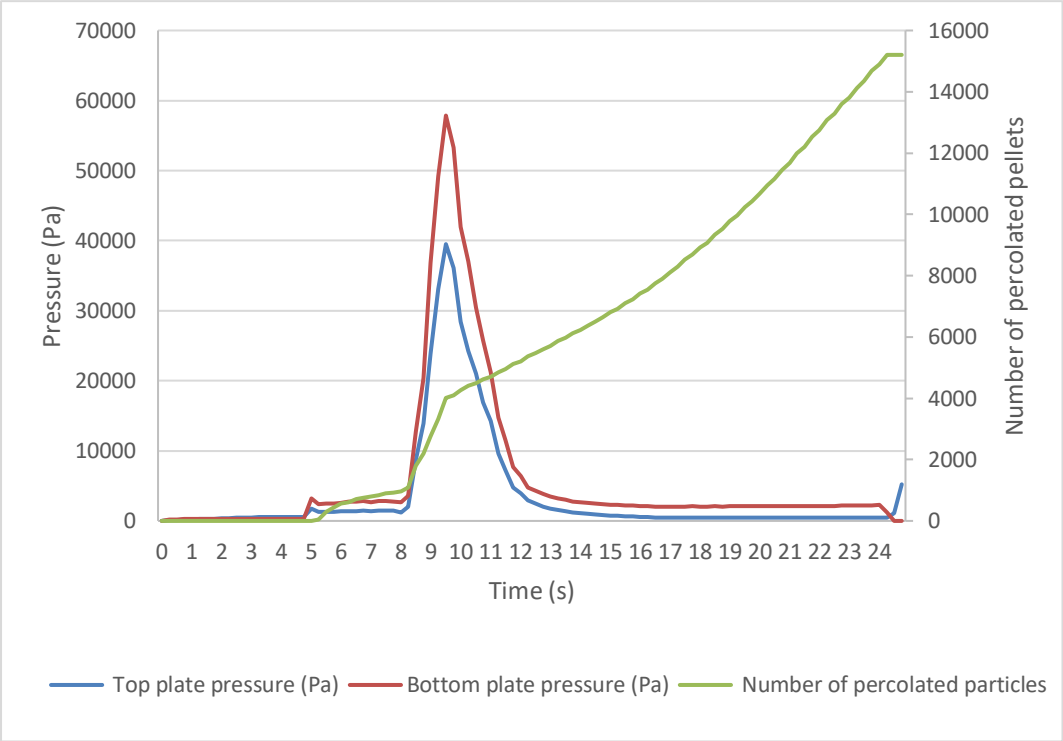

Figure 25: Cumulative number of percolated pellet particles (grey line), pressure on top (blue line) and bottom (orange line) of the system. Low-pressure case.

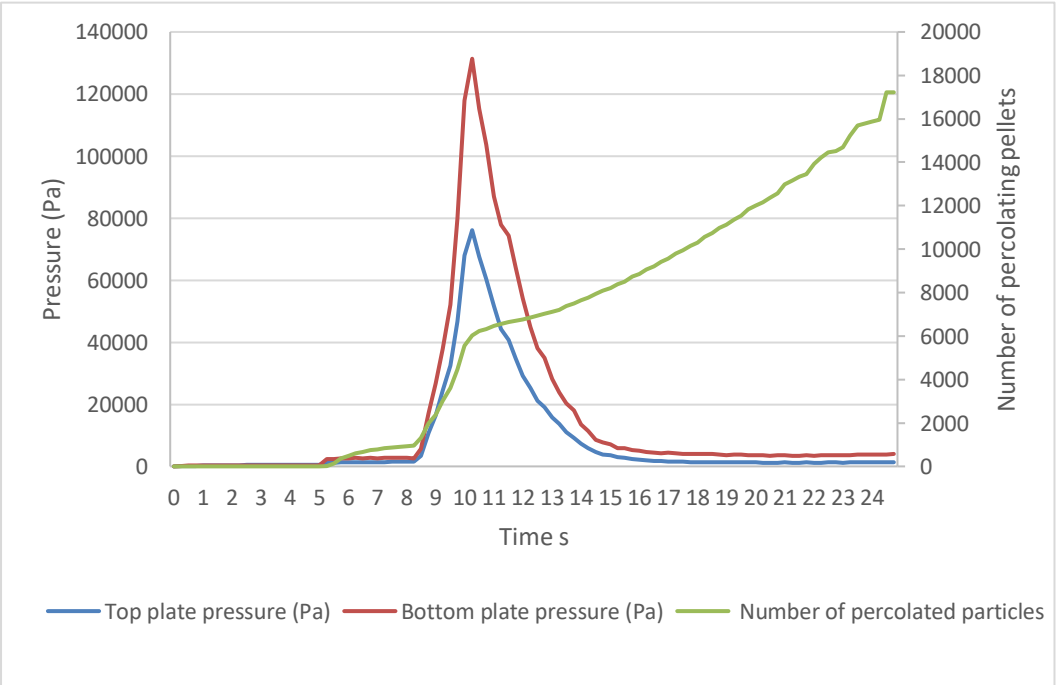

Figure 26: Cumulative number of percolated pellet particles (grey line), pressure on top (blue line) and bottom (orange line) of the system. High-pressure case.

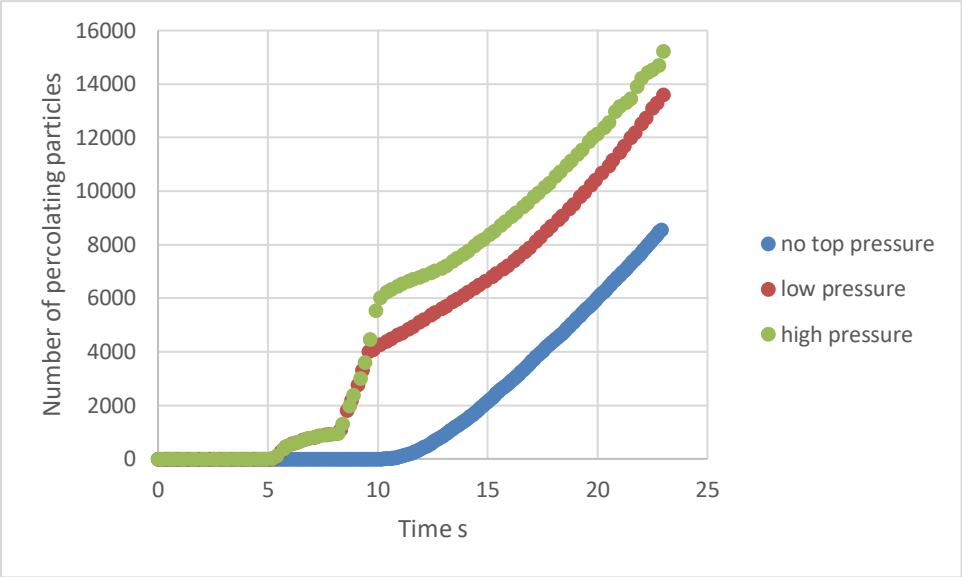

Figure 27: Number of percolating particles for different pressure level

Figure 28 shows that in the case of the no top pressure (no top plate), while for the case of low pressure there was a top place with downward velocity. The case of high pressure is similar to that of low pressure, BUT, in addition, material was generated on the top plate during descent which added extra pressure.

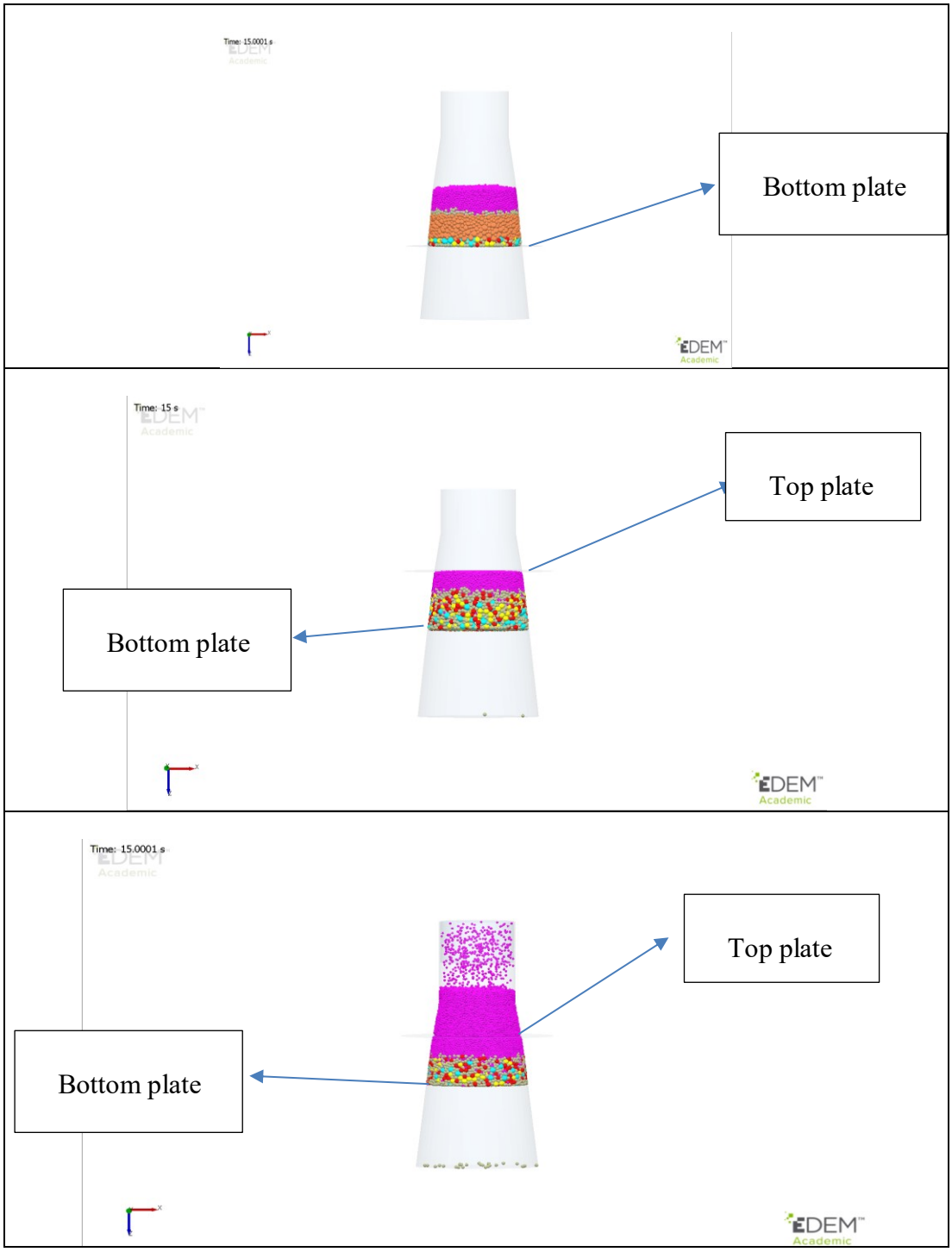

Figure 28: Setup for analysing the effect of pressure: Top: no pressure. Middle: low pressure. Bottom: high pressure.

6.2.2 Effect of Vibration

As a separate example, a small laboratory system was studied with beads of different size in a setup reminding of the layered structure encountered in the blast furnace. In this system, the bed was not descended due to practical constraint but was instead vibrated, since it is known that particle segregation and percolation can be triggered by vibration. Asmar et al. (2002), who studied segregation in a vibrated bed, observed little segregation at very low amplitude and high frequency. At low frequency and when the amplitude is high enough, segregation occurs but only in case the diameters of the particles differed sufficiently. At high values, the vibration frequency has little effect on the segregation. Hashemnia and Pourandi (2018) studied the effect of vibration frequency and amplitude percolation on a vibrated bed and concluded that the average velocity of particles inside the granular flow decreased as the vibration frequency increased, while it increased with increasing vibration amplitude. In the bed with low vibration frequencies, a bouncing flow mode was observed, while in the bed shaken with high frequencies the flows revealed abrupt jumps at the free surface and undulations (waviness) near their bottom walls. Esfandiary et al. (2013) observed that when the value of the dimensionless vibrational velocity was around two, the percolation became unsteady with the percolation velocity fluctuating in a wide range as a result of "crystallisation" in the vibrated bed, which abruptly increased the local packing density and decreased the particle percolation velocity significantly.

6.2.2.1 Laboratory Model

A small-scale laboratory model for studying particle percolation was constructed in a Bachelor's thesis work (Jansson, 2019). The system designed to study how smaller particles percolate through a bed of larger ones and was realised by placing glass beads on a grid mounted in a transparent plastic pipe (D = 143 mm), and a layer of smaller plastic balls (d_p = 6 mm) on top of the glass beads. The system was vibrated (at a frequency of 40-50 Hz), and the percolating small particles were led through a funnel and a hose to s scales, where the weight was registered. By this, the number of percolated particles could be followed in time. The system is illustrated in Figure 29. Since a size ratio of about 1:3 is needed for percolation, the underlying ("coke") bed was formed of a mixture of glass beads of two sizes ($d_{b,1}$ = 16 mm, $d_{b,2}$ = 25 mm). The density of all particles is in the range $\rho = 2.4\text{–}2.6\ \mathrm{g/cm^3}$.

Figure 29: Pilot model used for the experimental study of percolation. Left: Empty with grid mounted on the bottom. Right: Filled with particles.

A model roughly mimicking the experimental model was designed in EDEM, but the vibrations were deliberately exaggerated to reduce the computation time by increasing the amplitude significantly. Figure 30 shows the computational model and the state before and after an experiment. The (yellow) small particles that percolate through the bed were collected at the bottom and were registered by a “sampling box” at the outlet.

Figure 31 illustrates the results for a computational experiment with a bed of 2450 small plastic particles, as well as 195 and 65 medium-sized and large glass beads, respectively, for different vibration frequencies. From the results, a linear percolation rate was observed for low frequencies (10 Hz), but at higher frequencies (≥ 20 Hz) the process was fast, and all plastic particles eventually percolated through the bed. Furthermore, a frequency around 20 Hz was found to yield the maximum percolation rate, since higher or lower frequencies yielded slower percolation through the bed. Still, the differences are quite small. The increasing vibration may have increased collision and bouncing that, in turn, may have reduced the percolation rate due to energy dissipation.

In an analysis of the effect of the vibration amplitude, an amplitude of 0.6 cm was seen to produce the highest percolation rate, but increasing the value above 0.4 cm had a little overall impact on the percolation rate.

For the sake of comparison, experimental results form the laboratory rig are presented in Figure 32 for a set of ten experiments. The stochastic elements in the results are clearly seen, which is mainly due to the small number of glass beads and small ratio between the particle and bed diameters (d/D). However, the results for the simulated 10 Hz case shows similar overall features, even though the percolation rate is much more uniform (due to the larger amplitude of the vibrations, which makes the role of single channels less pronounced). It should also be noted that the large ("packing") particles moved considerably in the simulations, by contrast to the conditions in the laboratory experiments.

An advantage of the simulations compared to the experiments is that the internal structure of the bed can be studied in detail to gain a better understanding of the percolation phenomena. The left part of Figure 33 shows a bottom view of the system at a state during the percolation process, where the small (yellows) plastic particles about to percolate through the grid can be observed. Similar studies in the real system are difficult; the bed state at the end of a percolation experiment after dissection is presented in the right part of the figure.

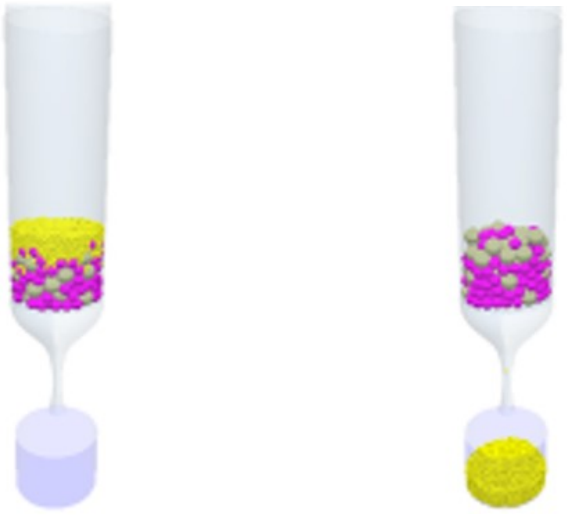

Figure 30: DEM-based model of the experimental model. Left: Situation before the start of percolation. Right: Situation after percolation.

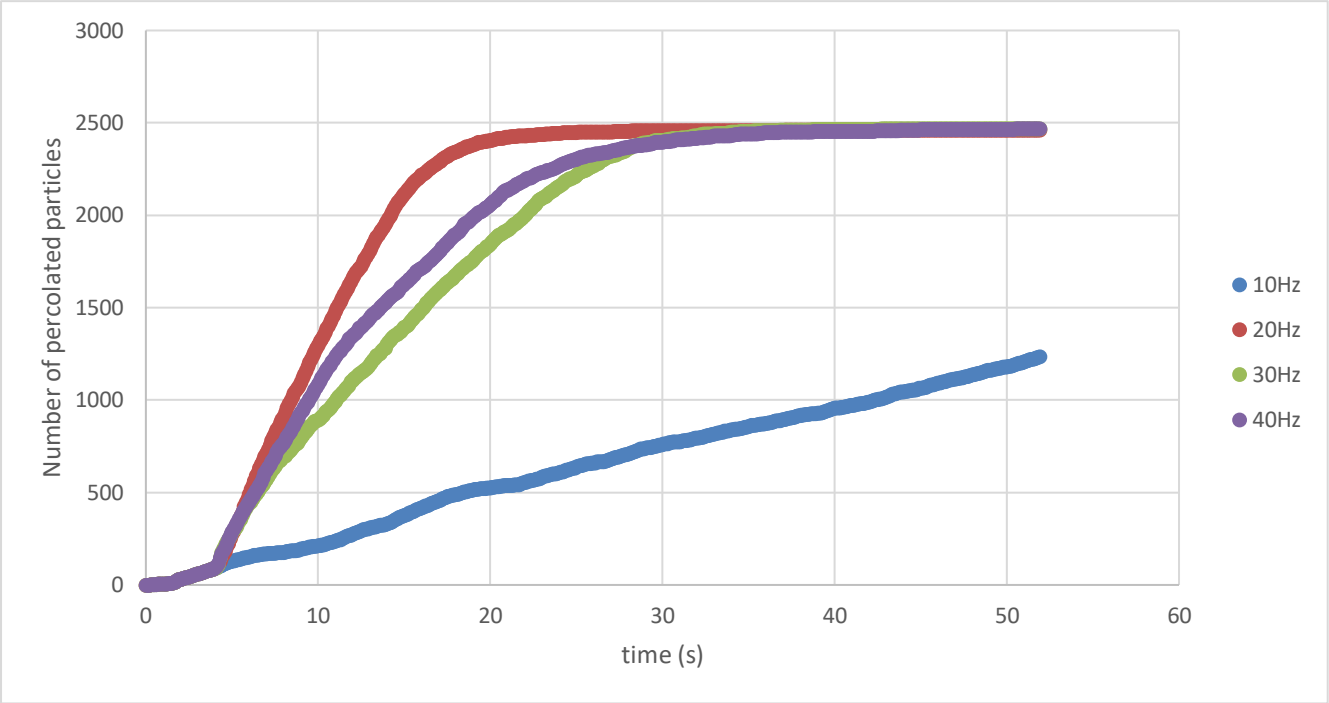

Figure 31: Cumulative number of percolating particles in the simulated laboratory model at different vibration frequencies.

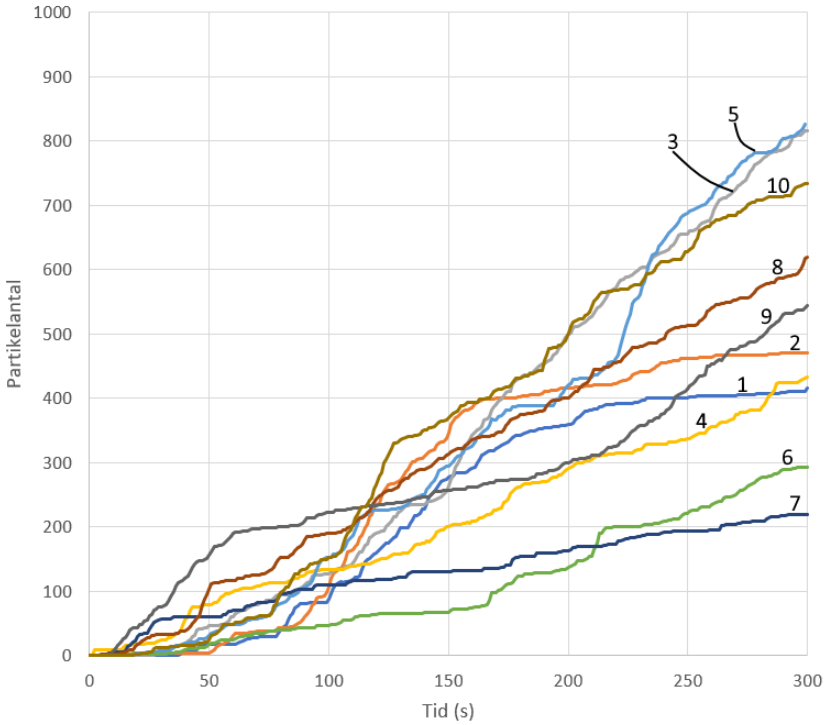

Figure 32: Cumulative number of percolating particles in the experimental laboratory model for ten runs under the same conditions (Jansson, 2019).

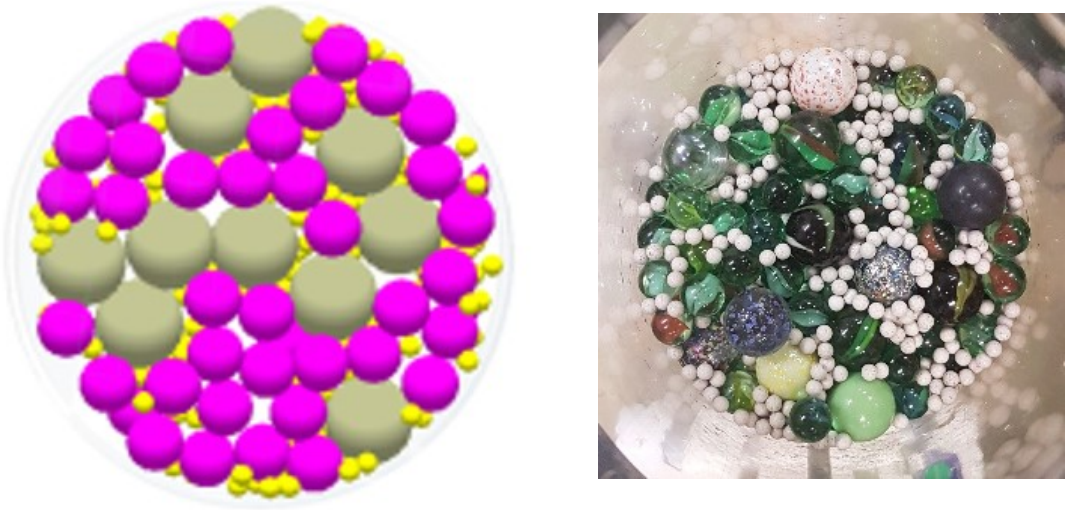

Figure 33: DEM-based model of the experimental model. Left: Situation before the start of percolation. Right: Situation after percolation

6.2.3 Silo with Repeated Charging and Discharging

As the final case studied in this work, a large pellet silo was simulated in considerably down-scaled form. The reason for studying the silo is that repeated charging and discharging of the pellet silos at SSAB Raahe had been found to yield problems with accumulated fines, which were purged when the level of the pellets in the silo descended below a critical limit, causing problems for the down-stream sieving and the blast furnace. The true dimensions of the silo are huge, so a dramatic reduction in size was needed to tackle the system computationally. In the examples to be presented first, the silo has a height and diameter of 1 m, respectively. A single square opening (size length 0.3 m) in the flat bottom acted as output (cf. bottom left schematic of Figure 8). Since fines cannot be simulated as they would yield millions of particles, equal numbers of particles of three sizes (d = 15 mm, 20 mm and 25 mm) were generated at charging, corresponding to a total number of about 76 000. Due to the size differences, the mass ratio of the particles are 12.5%, 29.6% and 57.9%. The particles were generated at the top, falling into the system filling it for about 7.5 s (except the first filling which took longer), followed by an

emptying cycle of around 4 s when the bottom opening was kept open. After this, it was closed, and the charging was repeated, followed by an emptying phase, repeating the procedure a number of time. The emptying time was chosen by trial and error to be such that the discharge was stopped just before the discharge hole was seen (from above). The simulated process is thus a simplification compared to the true process, where three silos operate, and the filling occurs for the "emptier" silo(s) as pellets arrive by ship. Figure 34 illustrates the simulated system during charging.

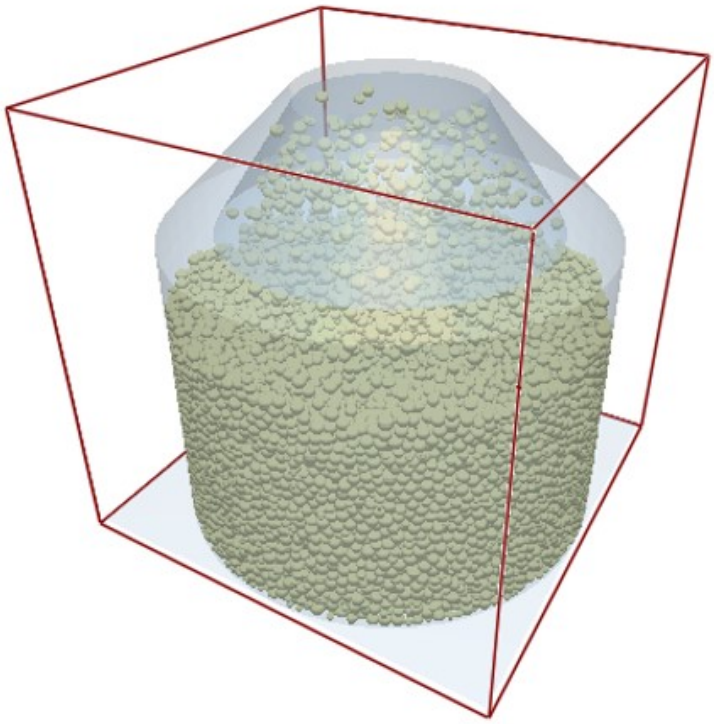

Figure 34: DEM-based model of the pellet silo. State at charging.

Seven charging-discharging cycles were simulated and the behaviour of the finest particle faction was studied. Figure 36 shows the evolution of the mass fraction of the finest particles in the entire silo. As the cycles are repeated, the mass fraction is seen to decrease, with clear local increases and decreases at charging and discharging. Unfortunately, the long computation time (about 14 days) did not allow for simulating more cycles, and the fraction is expected to decrease further. It means that more small particles are discharged than charged, possibly

because of their percolation towards the bottom through the bed of larger particles. This fact is also confirmed when the mass fraction of the smallest particles in the outflow stream is studied (Figure 37), which shows an increase even though a lot of stochastic variation is also observed.

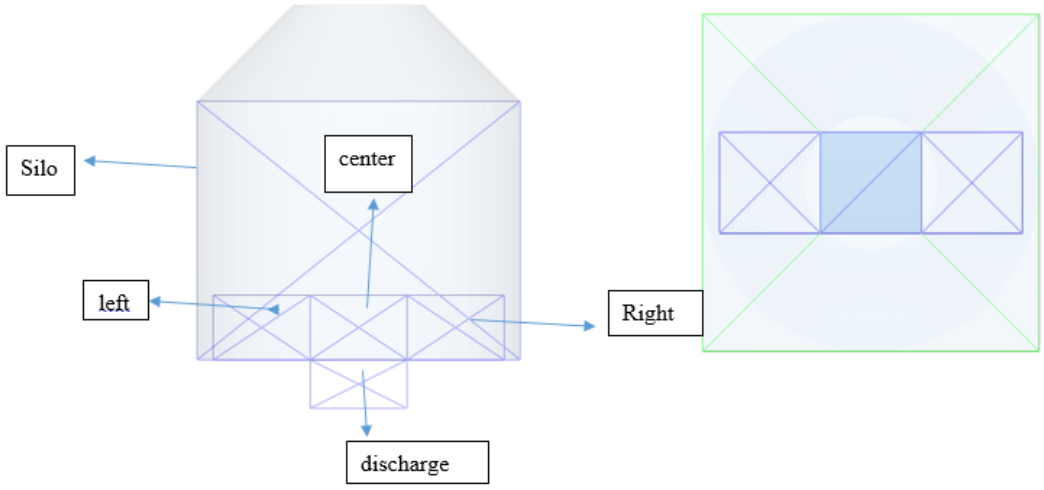

Figure 35: Image depicting front view (left) and top view (right) of virtual boxes for sampling in the silo with a single opening

The results in Figure 36 were obtained by dividing the mass of the smallest particle by the total mass of particles in the virtual box named “Silo” in Figure 35, while the results in Figure 37 were obtained by dividing the mass of the smallest particles by the total mass of particles in the virtual box named “discharge” in Figure 35.

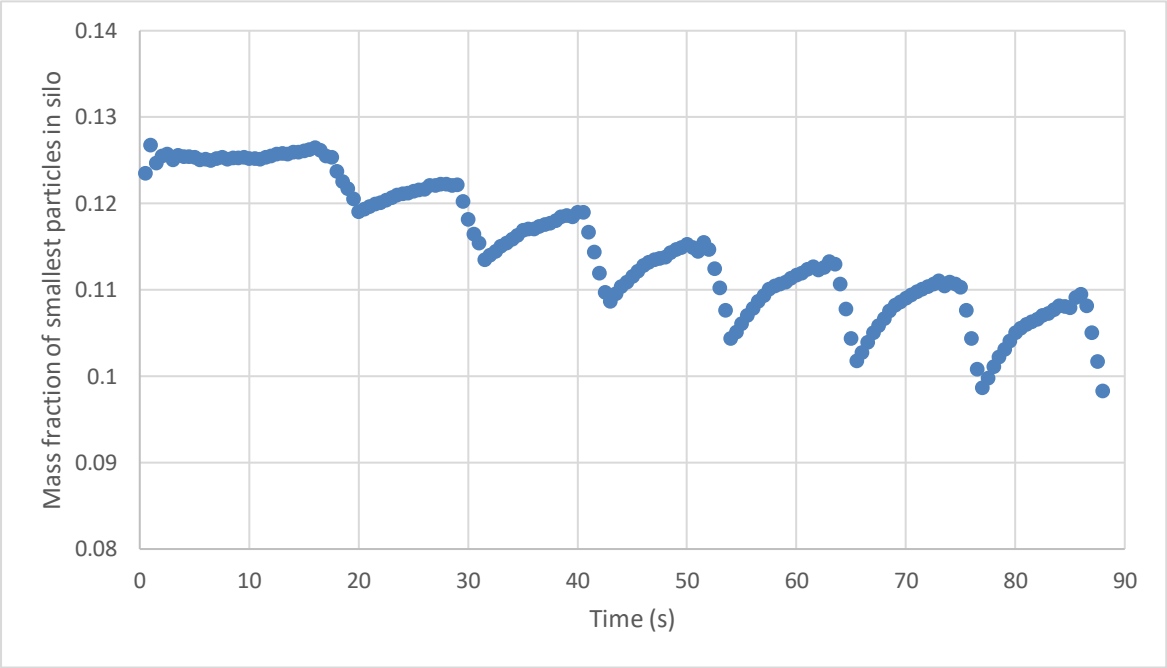

Figure 36: Mass fraction of the smallest particle size in the silo.

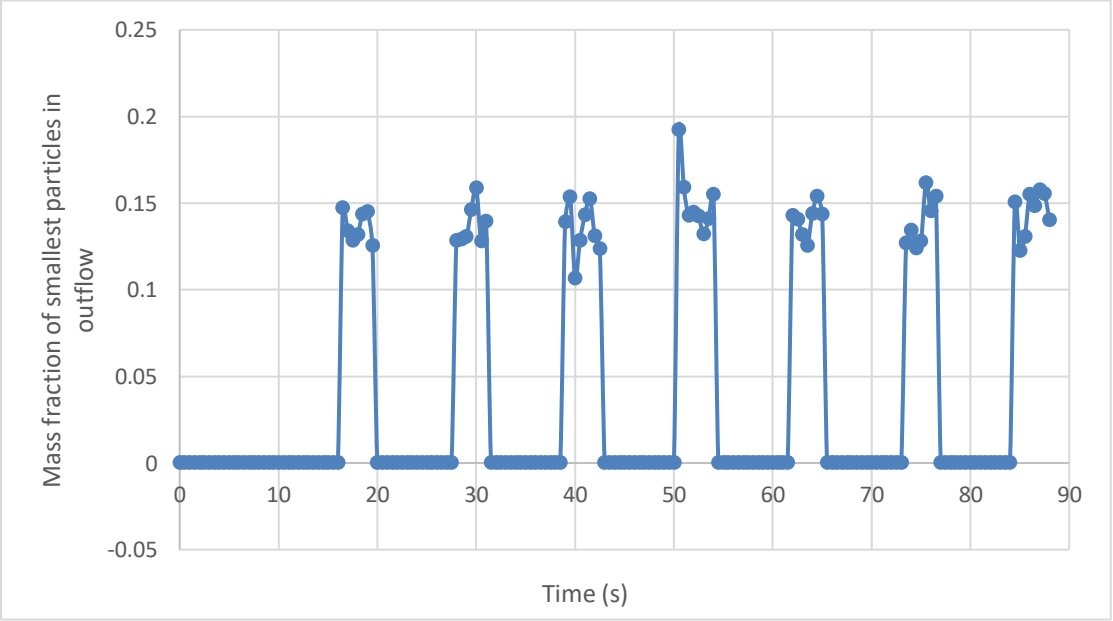

Figure 37: Mass fraction of the smallest particle size in the outflow from the silo.

It is also interesting to study the mass fraction of small particles at the bottom of the silo. Despite the overall depletion of the smallest particles in the silos, their share increases from 12.5% to above 13% during the seven cycles simulated (Figure 38), and the share is expected to show further increase if the simulation time could have been extended. As the silo is emptied, these small particles that have percolated down and are stored at the bottom will be discharged, substantially increasing the small fraction towards the end of the discharge.

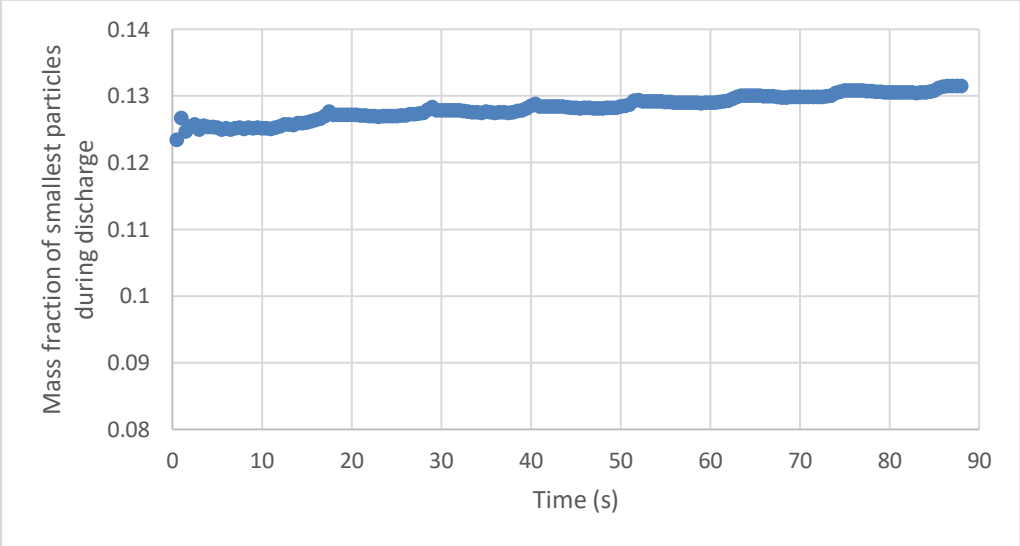

Figure 38: Mass fraction of the smallest particle size at the bottom of the silo.

The evolution of the mass fractions of the smallest particles at two sides of the only opening in the bottom is presented in Figure 39. They were obtained by dividing the mass of the smallest particle by the total mass of particles in the virtual box named “left” and “right” in Figure 35. The two fractions are seen to shows almost identical behaviour, as expected due to the symmetry, and exhibit a tooth-like increase and decrease along with the charging/discharging cycles. Thus, small particles accumulate in these regions, starting from a very low level. The low fractions in the starting point are due to particle segregation at filling, creating an initial bed of practically only large and medium-sized particles in the boxes.

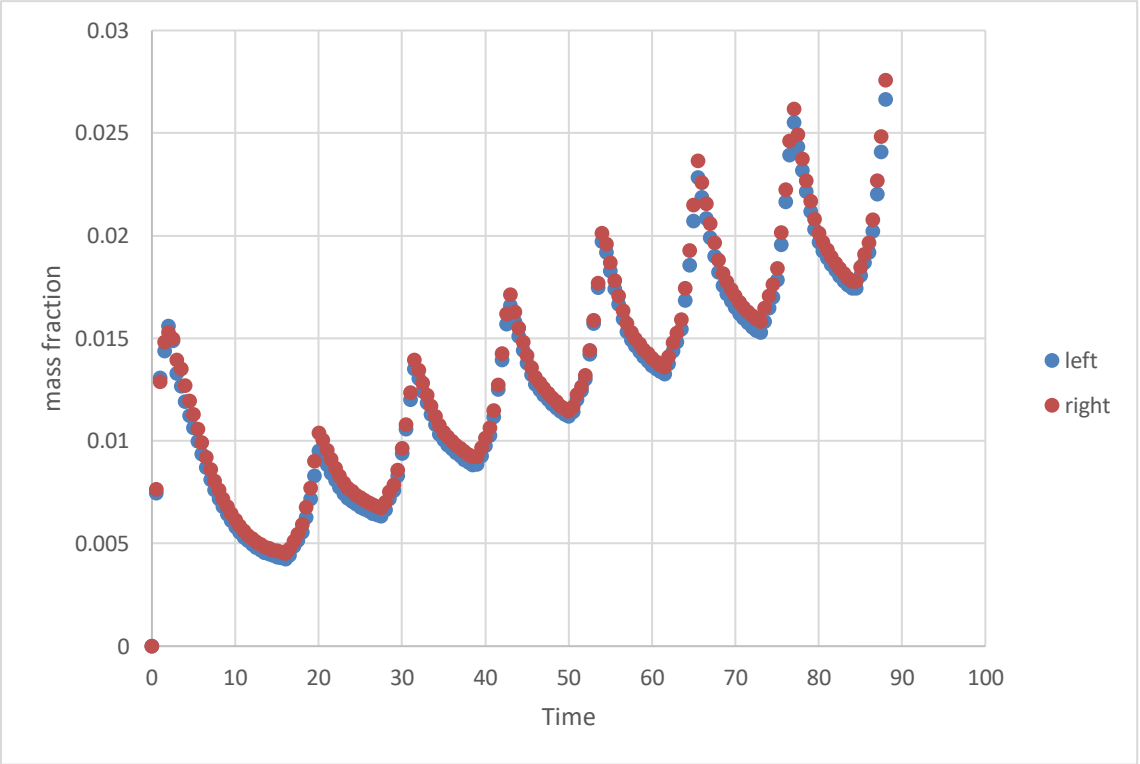

Figure 39: Small coke fraction at bottom vs. time in the laft and right "sampling boxes" (cf. Figure 35).

6.2.3.1 Silo with two and three openings

In an extension of the study, the geometry was made more realistic by including three bottom openings, just as in the true silo. To allow for this, the geometry had to be up-scaled. A silo diameter of 1.4 m and a height of 1.1 m were therefore used, while the openings were kept at the same size as in the study with one bottom hole. Virtual boxes under the openings were applied to record the characteristics of the outflows. For the case of operation with two openings, the center hole was closed (cf. left Figure 40, left panel).

Overall, the result obtained were similar to those for the silo with a single central hole, but the bed surface naturally showed more complicated patterns at charging and discharging. Despite the strong down-scaling, the simulated bed surface during discharge showed resemblance with imaging results from the real industrial silo, as seen in Figure 41.

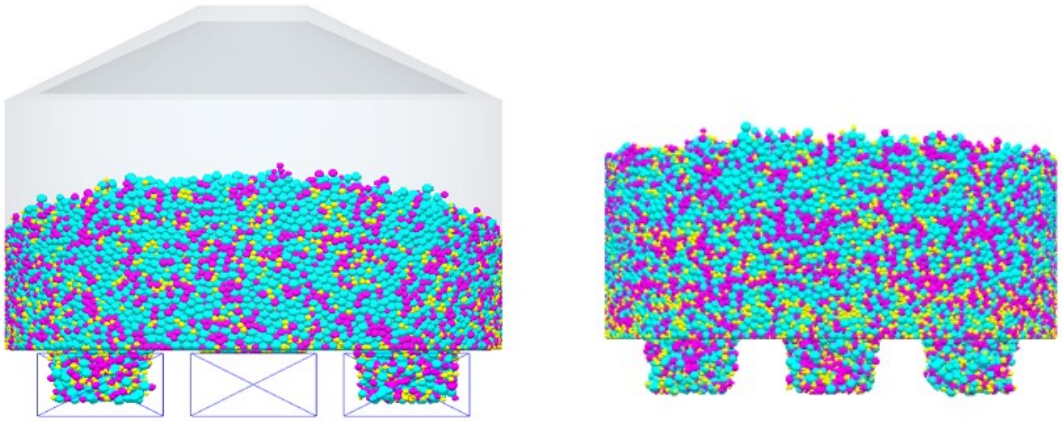

Figure 40: Front view of the larger silo with two (left) or three (right) openings

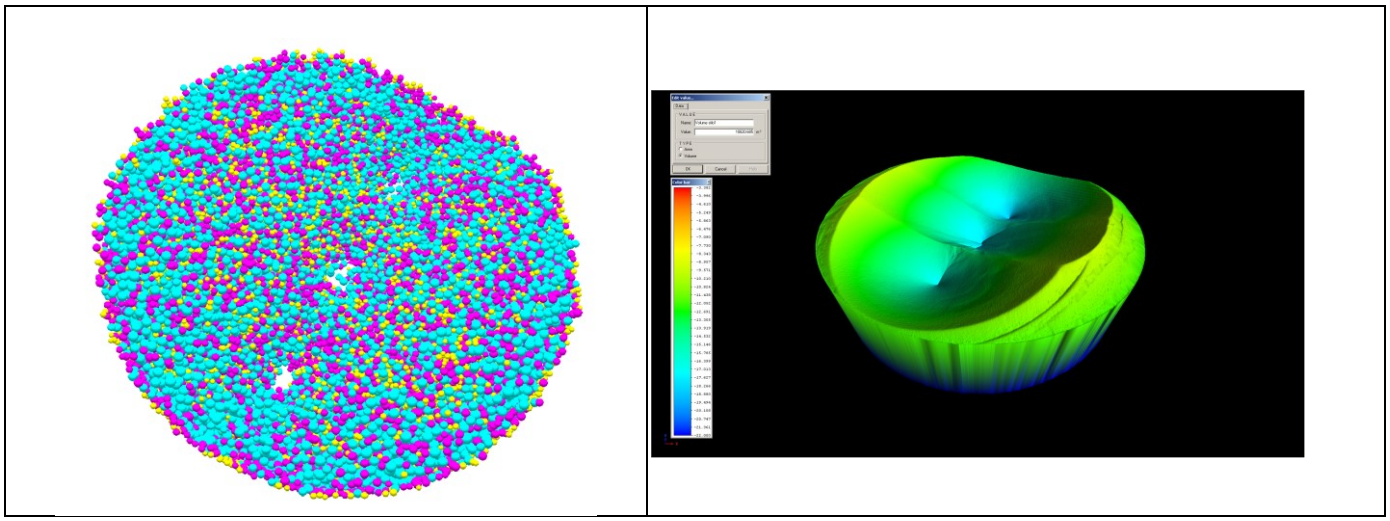

Figure 41: View of the simulated top surface of the particle bed in silo and results from laser scanner in the industrial counterpart.

Table 4: Number of particles in the silo after filling and discharge

Particle type	The average number at total fill		The average number when emptying stops	
	Two openings	Three openings	Two openings	Three opening
Big	60012	60711	26602	17058
Medium	62072	66442	26168	16430
Small	61715	80279	25453	18579
Total	183799	207432	78223	52067

7. CONCLUSIONS

This thesis has qualitatively and quantitatively studied percolation of smaller particles into beds of larger particle or particle mixtures for a set of tasks that are related to some problems encountered in the ironmaking industry. The two main tasks studied are percolation of pellets into (or through) underlying layers of coke and the behaviour of pellet fines in large pellet silos with discontinuous charging and discharging. These computational studies were based on the discrete element method (DEM). In all the cases, the systems studied had to be strongly down-scaled, which should naturally be kept in mind when the results are analysed.

For the descending system with a pellet layer residing on a coke layer, the smaller pellets were found to considerably penetrate the coke, filling the voids, particularly in the upper part of the layers. In a geometry that expands, like the shaft in the blast furnace, the percolation rate increases due to new voidage formed as the layers expand horizontally. It counteracts the strong wall effect observed in the cylindrical (non-expanding) system, where particularly the coke-layer descent was retarded by friction against the wall. Logically, a larger expansion (more conical shaft) yields faster percolation. Also, the percolation rate increased with the descent rate of the layers. As for the effect of particle properties, the size ratio between the small and large particles played a major role, while the effects of static and rolling friction were less important.

A brief computational study of a small-scale laboratory model developed in a parallel B.Sc. work was also undertaken, yielding findings in general agreement with the experimental ones. However, the stronger vibration used in the computational analysis (to speed up the calculations) made the systems somewhat different.

In the silo simulations, the behaviour of small particles (“fines”) in a system with intermittent charging and discharging exhibited complex behaviour, where spatial distributions change with time in a non-linear way. Even though the results are preliminary, they suggest that a more regular filling of the different silos, keeping the levels more constant, could yield less time-dependent patterns in the outflows.

Finally, it may be concluded that even though there are still several shortcomings in the use of DEM for studying industrial problems, the technique has been shown to be a resourceful tool in the analysis of the complex flow of particulate matter.

REFERENCES

Anjani, J. **(2008)**. Percolation segregation in multi-size and multicomponent particulate mixtures: measurement, sampling, and modeling. *PhD Dissertation*. Pennsylvania State University, PA, USA.

Ariyama, T., Natsui, S., Kon, T., Ueda, S., Kikuchi, S. and Nogami, H**. (2014)**. Recent Progress on Advanced Blast Furnace Mathematical Models Based on Discrete Method. *ISIJ International*, 54(7), pp. 1457-1471.

Asmar, B., Langston, P. and Matchett, A. **(2002)**. A generalised mixing index in distinct element method simulation of vibrated particulate beds. *Granular Matter*, 4(3), pp. 129-138.

Bertrand, F., Leclaire, L. and Levecque, G. **(2005)**. DEM-based models for the mixing of granular materials. *Chemical Engineering Science*, 60(8-9), pp. 2517-2531.

Bridgwater, J. and Ingram, N.D. **(1971)**. Rate of spontaneous inter-particle percolation. *Trans. Inst. Chem. Engineer*, 49, pp. 163–169.

Bridgwater, J., Cooke, M.H. and Scott, A.M. **(1978)** Inter-particle percolation: equipment development and mean percolation velocities, *Trans. Inst. Chem. Engineer*, Vol. 56, pp. 157–167.

Bridgwater, J., Foo, W.S. and Stephens, D.J. **(1985)**. Particle mixing and segregation in failure zones – theory and experiment. *Powder Technology*, Vol. 41, pp. 147–158.

Chou, C., Lee, A., Yeh C. **(2009)**. Placement of a non-isosceles-triangle insert in an asymmetrical two-dimensional bin-hopper. *Advanced Powder Technology*, 20, pp. 80-88

Combarros, M., Feise, H., Zetzener, H. and Kwade, A. **(2014)**. Segregation of particulate solids: Experiments and DEM simulations. *Particuology*, 12, pp. 25-32.

Cundall, P. A. and Strack O. D. L. **(1979)**. A discrete numerical model for granular assemblies. *Geotechnique*, 29(1), pp. 47-65.

DEM Solutions Ltd. **(2016)**. EDEM 2017 User Guide. Copyright © 2016.

Dutt, M.,Elliott, A.E. **(2014)**. Granular dynamics simulations of the effect of grain size dispersity on uniaxially compacted powder blends. *Granul. Matter*, 16, pp. 243–248.

Džiugys, A. and Navakas, R**. (2009)**. The role of friction in mixing and segregation of granular material. *Granular Matter*, 11(6), pp. 403-416.

Džiugys, A. and Peters, B. **(2001)**. An approach to simulate the motion of spherical and non-spherical fuel particles in combustion chambers. *Granular Matter*, 3(4), pp. 231-266.

Engblom, N., Saxén, H., Zevenhoven, R., Nylander, H. and Enstad, G. **(2012)**. Effects of process parameters and hopper angle on segregation of cohesive ternary powder mixtures in a small scale cylindrical silo. *Advanced Powder Technology*, 23(5), pp.566-579.

Esfandiary, A., Dong, K. and Yu, A. **(2013)**. Formation of ordered structure and its effect on particle percolation in a vibrated bed. *AIP Conference Proceedings*, 1542, 747

Fan, Y., Boukerkour, Y., Blanc, T., Umbanhowar, P., Ottino, J. and Lueptow, R. **(2012)**. Stratification, segregation, and mixing of granular materials in quasi-two-dimensional bounded heaps. *Physical Review E*, 86(5), 051305.

Geerdes, M., Chaigneau, R. and Kurunov, I. **(2015)**. *Modern Blast Furnace Ironmaking*. Burke: IOS Press.

Guha, M., Nag, S., Kundu, S., Patra, M., Sinha, S. and Kumar, S. **(2009)**. Particle Size Segregation in the Falling Stream of Burden Materials. *ISIJ International*, 49(11), pp. 1816-1818.

Guo, Y., Wu, C., Kafui, K. and Thornton, C. **(2011)**. 3D DEM/CFD analysis of size-induced segregation during die filling. *Powder Technology*, 206(1-2), pp. 177-188.

Hashemnia, K. and Pourandi, S. **(2018)**. Study on the effect of vibration frequency and amplitude on the quality of fluidisation of a vibrated granular flow using discrete element method. *Powder Technology*, 327, pp. 335-345.

Hashim, MHM, Sharrock, GB & Saydam, S. **(2008).** A Review of Particle Percolation in Mining. In Potvin, Y, Carter, J., Dyskin, A. and Jeffrey, R. (Eds.), *Proceedings of the First*

Southern Hemisphere International Rock Mechanics Symposium, Australian Centre for Geomechanics, Perth, pp. 273-284.

Jha, A. and Puri, V. **(2011)**. Percolation Segregation in Binary Size Mixtures under Different Shear and Intensity of Motion. *Particulate Science and Technology*, 29(5), pp. 481-492.

Jansson, R. **(2019)**. Undersökning av partikelperkolation med experiment och simulering (Investigation of particle percolation with experiments and simulation). B.Sc. thesis, Thermal and Flow Engineering Laboratory, Åbo Akademi University, Finland.

Johanson, K. **(2014).** Review of new segregation tester method by Dr Kerry Johanson, P.E. *Powder Technology*, 257, pp. 1-10.

Ketterhagen, W., Curtis, J., Wassgren, C. and Hancock, B. **(2008)**. Modelling granular segregation in flow from quasi-three-dimensional, wedge-shaped hoppers. *Powder Technology*, 179(3), pp. 126-143.

Ketterhagen, W., Curtis, J., Wassgren, C. and Hancock, B. **(2009)**. Predicting the flow mode from hoppers using the discrete element method. *Powder Technology*, 195(1), pp. 1-10.

Kou, M., Wu, S., Du, K., Shen, W., Sun, J. and Zhang, Z. **(2013)**. DEM Simulation of Burden Distribution in the Upper Part of COREX Shaft Furnace. *ISIJ International*, 53(6), pp. 1002-1009.

Langston, P., Al-Awamleh, M., Fraige, F. and Asmar, B. **(2004).** Distinct element modelling of non-spherical frictionless particle flow. *Chemical Engineering Science*, 59(2), pp. 425-435.

Li, H. **(2005)**. *Impact of cohesion forces on particle mixing and segregation*. PhD thesis, School of Engineering, University of Pittsburgh, PA, USA.

Li, J., Yu, A., Bridgwater, J. and Rough, S. **(2010)**. Spontaneous inter-particle percolation: A kinematic simulation study. *Powder Technology*, 203(2), pp. 397-403.

Li, Y., Xu, Y., Jiang S. **(2008)**. DEM simulations and experiments of pebble flow with monosized spheres. *Powder Technology*, 193, pp. 312-318

Lommen, S., Schott, D. and Lodewijks, G. **(2014)**. DEM speedup: Stiffness effects on behaviour of bulk material. *Particuology*, 12, pp. 107-112.

Matsuhashi, S., Kurosawa, H., Natsui, S., Kon, T., Ueda, S., Inoue, R. and Ariyama, T. **(2012)**. Evaluation of Coke Mixed Charging Based on Packed Bed Structure and Gas Permeability Changes in Blast Furnace by DEM-CFD Model. *ISIJ International*, 52(11), pp. 1990-1999.

Mio, H., Komatsuki, S., Akashi, M., Shimosaka, A., Shirakawa, Y., Hidaka, J., Kadowaki, M., Matsuzaki, S. and Kunitomo, K. **(2009).** Effect of Chute Angle on Charging Behavior of Sintered Ore Particles at Bell-less Type Charging System of Blast Furnace by Discrete Element Method. *ISIJ International*, 49(4), pp. 479-486.

Mitra, T. **(2016)**. Modelling of burden distribution in the blast furnace. PhD Thesis, Thermal and Flow Engineering Laboratory, Åbo Akademi, Finland.

Mosby, J., de Silva, S. and Enstad, G. **(1996)**. Segregation of Particulate Materials – Mechanisms and Testers. *KONA Powder and Particle Journal*, 14(0), pp. 31-43.

N. Engblom, H. Saxén, R. Zevenhoven, H. Nylander, G. G. Enstad. **(2012)** Segregation of Construction Materials in Silos. Part 2: Identification of Relevant Segregation Mechanisms. *Particulate Science and Technology*, 30:2, pp. 161-178.

Nag, S., Guha, M., Kundu, S., Sinha, S. and Singh, U. **(2008)**. Mass Distribution in the Falling Stream of Burden Materials. *ISIJ International*, 48(9), pp.1316-1318.

Pierce, M. **(2004)**. PFC3D modelling of inter-particles percolation in caved rock under draw. Numerical modelling in micromechanics via particle methods. *Proceedings of the 2nd International PFC Symposium* (Eds. Shimizu, Y., Hart, R. and Cundall, P.), London, Taylor and Francis Group, pp. 149–156.

Qiu, J., Ju, D., Zhang, J. and Xu, Y**. (2017)**. DEM simulation of particle flow in a parallel-hopper bell-less charging apparatus for blast furnace. *Powder Technology*, 314, pp. 218-231.

Rahman, M., Zhu, H., Yu, A. and Bridgwater, J. **(2008)**. DEM simulation of particle percolation in a packed bed. *Particuology*, 6(6), pp. 475-482.

Remond, S. **(2010)**. DEM simulation of small particles clogging in the packing of large beads. *Physica A: Statistical Mechanics and its Applications*, 389(21), pp. 4485-4496.

Sakaguchi, E., E. Ozaki, and T. Igarashi. **(1993)**. Plugging of the flow of granular materials during the discharge from a silo. *Int. J. Mod. Phys. B* 7, pp. 1949-1963.

Scott, A. and Bridgwater, J. **(1975)**. Interparticle Percolation: A Fundamental Solids Mixing Mechanism. *Industrial & Engineering Chemistry Fundamentals*, 14(1), pp. 22-27.

Takahashi, H., Kushima, K. and Takeuchi, T. **(1989)**. Two-dimensional analysis of burden flow in blast furnace based on plasticity theory. *ISIJ International*, 29(2), pp. 117-124.

Tang, P. and Puri, V. **(2005)**. An Innovative Device for Quantification of Percolation and Sieving Segregation Patterns–Single Component and Multiple Size Fractions. *Particulate Science and Technology*, 23(4), pp. 335-350.

Ueda, S., Natsui, S., Nogami, H., Yagi, J. and Ariyama, T. **(2010)**. Recent Progress and Future Perspective on Mathematical Modeling of Blast Furnace. *ISIJ International*, 50(7), pp. 914-923.

Wei, H., Zhao, Y., Zhang, J., Saxén, H. and Yu, Y. **(2017)**. LIGGGHTS and EDEM application on charging system of ironmaking blast furnace. *Advanced Powder Technology*, 28(10), pp. 2482-2487.

Wu, J., Binbo, J., Chen, J., Yang, Y. **(2009)**. Multi-scale study of particle flow in silos. *Advanced Powder Technology*, 20, p. 62

Xiao, H., Umbanhowar, P., Ottino, J. and Lueptow, R. **(2016)**. Modelling density segregation in flowing bidisperse granular materials. *Proceedings of the Royal Society A: Mathematical, Physical and Engineering Science*, 472(2191), p. 20150856.

Xu, J., Hu, Z., Xu, Y., Wang, D., Wen, L. and Bai, C. **(2017)**. Transient local segregation grids of binary size particles discharged from a wedge-shaped hopper. *Powder Technology*, 308, pp. 273-289.

Tsuji, Y., Tanaka, T. and T. Ishida, T. **(1992)**. Lagrangian numerical simulation of plug flow of cohesionless particles in a horizontal pipe. *Powder Technology*, 71, pp. 239-250.

Yu, Y. and Saxén, H. **(2010)**. Experimental and DEM study of segregation of ternary size particles in a blast furnace top bunker model. *Chemical Engineering Science*, 65(18), pp. 5237-5250.

Yu, Y. and Saxén, H. **(2011)**. Discrete element method simulation of properties of a 3D conical hopper with mono-sized spheres. *Advanced Powder Technology*, 22(3), pp. 324-331.

Yu, Y., A. Westerlund, T. Paananen and H. Saxén. **(2011)**. Inter-particle percolation segregation during burden descent in the blast furnace. *ISIJ International* 51, pp. 1050-1056.

Yu, Y. and Saxén, H. **(2012)**. Effect of DEM Parameters on the Simulated Inter-particle Percolation of Pellets into Coke during Burden Descent in the Blast Furnace. *ISIJ International*, 52(5), pp. 788-796.

Yu, Y. and Saxén, H. **(2014)**. Segregation behaviour of particles in a top hopper of a blast furnace. *Powder Technology*, 262, pp. 233-241.

Zhang, T., Gan, J., Pinson, D. and Zhou, Z. **(2018)**. Size-induced segregation of granular materials during filling a conical hopper. *Powder Technology*, 340, pp. 331-343.

Zhu, H. and Yu, A. **(2005)**. Micromechanic modelling and analysis of unsteady-state granular flow in a cylindrical hopper. *Journal of Engineering Mathematics*, 52(1), pp. 307-320.

Zhu, H. and Yu, A. **(2005)**. Steady-state granular flow in a 3D cylindrical hopper with flat bottom: macroscopic analysis. *Granular Matter*, 7(2-3), pp. 97-107.

Zhu, H., Rahman, M., Yu, A., Bridgwater, J. and Zulli, P. **(2009)**. Effect of particle properties on particle percolation behaviour in a packed bed. *Minerals Engineering*, 22(11), pp. 961-969.

Zhu, H., Zhou, Z., Yang, R. and Yu, A. **(2007)**. Discrete particle simulation of particulate systems: Theoretical developments. *Chemical Engineering Science*, 62(13), pp. 3378-3396.

Zhu, H., Zhou, Z., Yang, R. and Yu, A. **(2008)**. Discrete particle simulation of particulate systems: A review of major applications and findings. *Chemical Engineering Science*, 63(23), pp. 5728-5770.